단층 운동시 댐 파괴 거동 해석

Crack Propagation in Earth Embankment
Subjected to Fault Movement.

손 준 익 박사

(한국건설기술연구원, 선임연구원)

Crack Propagation in Earth Embankment
Subjected to Fault Movement

by Joonik Sohn

ABSTRACT

Model studies on the response of homogeneous earth embankment dams subjected to
strike-slip fault movement have been performed via centrifuge and finite element
analysis. The centrifuge model tests have shown that crack development in earth
embankments experiences two major patterns: shear failure deep inside the embankment
and tension failure near the surface. The shear rupture zone develops from the base
level and propagates upward continuously in the transverse direction but allows no
open leakage channel. The open tensile cracks develop near the surface of the
embankment, but they disappear deep in the embankment. The functional relationship
has been developed based on the results of the centrifuge model tests incorporating
the variables of amount of fault movement, embankment geometry, and crack propagation
extent in earth dams. This set of information can be used as a guide line to
evaluate a "transient" safety of the damaged embankment subjected to strike-slip
fault movement.

The finite element analysis has supplemented the additional explanations on
crack development behavior identified from the results of the centrifuge model tests.
The bounding surface time-independent plasticity soil model was employed in the
numerical analysis. Due to the assumption of continuum in the current version of the
3-D FEM code, the prediction of the soil structure response beyond the failure
condition was not quantitatively accurate. However, the fundamental mechanism of
crack development was qualitatively evaluated based on the stress analysis for the
deformed soil elements of the damaged earth embankment. The tensile failure zone is
identified when the minor principal stress of the deformed soil elements less than
zero. The shear failure zone is identified when the stress state of the deformed

soil elements is at the point where the critical state line intersects the bounding surface.

INTRODUCTION

Evaluation of the ability of earth embankments to withstand safely the effects of earthquakes has been a continuing issue in the geotechnical engineering during the past thirty years or so. The principal actions of an earthquake which endanger the safety of a dam can be classified largely in two catagories: faulting and the attendant permanent deformations of the earth crust, and shaking of the foundation and dam together with the associated acceleration forces. The causes of dam instability due to the dynamic response of earthquake acceleration have been widely studied and well identified: the failure of embankment slopes due to earthquake loadings; the excessive embankment deformation and/or crest settlement resulting from the seismic mobility; and liquefaction of embankment as well as foundation soils. However, dam breakage due to fault movement in the foundation has not been extensively studied, even though its potential hazards are just as severe if not more than the others. One possible reason for the lack of concern of this problem could be that many engineers perceive that there is little probability for the existance of this type of failure. The other possibility could be that some dam designers have assumed that the relative displacement of the fault is generally too small to make any change in the design, thus they neglect it.

While fault movement is a relatively infrequent cause of damage to any kind of structure, it probably constitutes a more serious threat to dams than to any other classes of engineering structures. Fault displacement of large magnitude can cause sudden surface ruptures of a few feet to tens of feet. If the water in the reservoir were suddenly released as a result of breakage or failure of the dam, damages to the

downstream areas could be devastating. In addition, there is a greater likelihood that dams will be located over faults, both because of the relatively great length of a dam and because of the frequent coincidence of faults and river valleys. In many parts of the world, including much of California, an appreciable fraction of the main river and stream valleys on which dams are normally built have developed along faults. The San Andreas Fault in California is a classic and probably the most intensely studied example. Table 1 is a partial list compiled by Bennett (1985) of embankment dams in California located on active faults. Some of them are situated precariously above densely populated areas. Should there be a dam failure due to fault movement, the consequences of potential damage are indeed awesome.

To date, the design practice for dam breakage due to fault movement is largely empirical, stressing the importance of a proper choice of design details, such as a transition zone, to ensure safety against rupture (Sherard et al., 1974). The guidelines suggested are based upon related field performances of a limited number of dams subjected to fault movement in the foundation and upon the judgement of experienced dam designers. Little of this information, however, can be quantified to form the basis of a general and yet practical procedure for evaluating the safety of existing or proposed embankment dams.

For the present research, both physical modeling via the centrifuge and numerical modeling via the finite element technique were carried out for a homogeneous earth embankment dam subjected to fault movement. The objectives of this research are to identify the possible failure mechanisms and crack patterns using the information provided by the centrifuge model tests; to compare the model dam behavior with numerical prediction; to suggest a practical guideline to be used for safe design of dams establishing a functional relationship between the amount of fault movement, embankment geometry and the crack propagation extent in earth dams.

As fault movement usually occurs during a strong earthquake, the overall seismic stability of an embankment dam is very complex. The above mentioned causes of dam instabilities could also be complicated due to site conditions. In this research, however, the fault movement action is isolated from the complex conditions thus focusing the study of crack development due only to the abrupt base movement. It should be noted that the type of fault considered in this research is the "strike-slip" fault, thus the conclusions included herein are not pertinent to damages caused by other types of faulting.

FAULT

Faults are fractured surfaces in crustal strata along which the adjacent bedrock has been displaced, involving relative movement of the two sections of the fractured rock. These are formed in relief of stress which has accumulated in rocks undergoing tectonic deformation. The earthquake is an expression of release of such pressures exerted upon bed rocks. When the earth crust is subjected to great pressure, it has to withstand the shear forces developed as a result of compression or tension. If the shear stress becomes greater than the shear strength along the future failure plane of the crust, failure will result; movement will take place along the plane of failure until an equilibrium state of the forces is reestablished. The relative movements between the walls of a fault during an earthquake may be primarily vertical (dip-slip) or horizontal (strike-slip), depending on the local stress system in the earth's crust that caused the earthquake.

Faults are generally formed in three different patterns, namely trust faults, normal faults, and strike-slip or wrench faults. Where the dominant compression is horizontal and the vertical load is small, shear fractures will form as shown in Figure 1(a), and faults having this kind of orientation are the thrusts or thrust

faults. These involve vertical displacements caused by horizontal compression. Where both the maximum and minimum stresses are horizontal and the intermediate stress vertical (Figure 1(b)), the resulting fractures are vertical surfaces forming strike-slip or wrench faults. These involve primarily horizontal displacements. Thirdly, where the greatest stress is vertical (Figure 1(c)), the shear planes are steeply inclined to the horizontal and faults formed under such stress conditions are normal faults. These involve vertical displacements caused by horizontal extension. They are less frequently found than the other fault types.

The nature of ground fracturing caused by displacements of the three types of faults varies markedly, and has very significant engineering ramifications. Since the strike-slip fault causes primarily horizontal displacements, there is no consistent tendency for the ground on one side to be higher than the other side. Therefore, it is more common that streams may be captured by the fault and follow along it creating a long narrow valley. For the thrust and normal faults, which generally cause a consistent change in the relative elevation of the ground on opposite sides, the fault commonly runs along a contour on the lower slope of a hill or mountain. For these faults therefore, it is not common for a stream or river to follow the fault for any distance. The stream coming out of the hills may cross the faults or may run parallel to the fault at a lower elevation.

The amount of fault rupture may vary from only a few centimeters to many kilometers. One of the most notable examples of lateral rupture is along the San Andreas fault in California totalling over 640 km (Bell, 1983). However the relative movement of the break for a given earthquake event have ranged from only a few millimetres to a maximum of the order of 10 m. It is particularly important to trace the fault as far as possible and to estimate its probable length of rupture, in order to guide the estimate of the displacement (relative movement) which might occur

along the fault.

A number of investigators have compiled statistics regarding fault breaks in historic time. According to Sherard et al. (1974), the ratio of average to maximum displacement ranged roughly between 0.2 and 0.7 with an average of about 0.4, which also shows that for the great majority of fault breaks, the maximum displacement was less than 5 or 6 m. The average displacement along the length of break was less than 50 % of the maximum. These figures suggest the probability of confidence for building safe embankment dams at sites with active faults. Generally, the values of offset displacement accepted for the conservative design of a embankment dam are less than 3 m and a practical maximum is of the order of 7 to 8 m.

There is a rough relationship in observed historic fault breaks between the length of fault break and the amount of fault movement, which is related to the magnitude of the earthquake. Figure 2 showing these relationships, prepared by Bonilla (1970), is used as a guide to judgement in predicting the maximum displacement on a given fault.

PART A : CENTRIFUGE MODEL STUDY

A1. INTRODUCTION

The centrifuge model study gives us the opportanity to see a failure, which might lead to a relevant approach to solve a problem. This model study can provide us with informations to identify the possible important factors that may have significant bearings on the response of the dam and subsequent rupture potential during and after fault movement. The purpose of this research is to identify the failure mechanism of dam breakage due to fault movement, and further develop a practical guide line to be used for safe dam design from the parametric study between the amounts of fault movement, embankment geometry and the crack development in earth dams.

A2. CENTRIFUGE TESTING

A small scale laboratory model is severely limited in its applicability to the prediction of behavior of the full scale geotechnical structure, because when gravity is the principal loading agent, the stress state in a small scale model loaded by its own weight is much smaller in magnitude than in the corresponding full scale prototype. This difference in stress state gives model behavior quite different from that of the prototype because soil properties are stress dependent. However, if the model is placed in a centrifuge and subjected to centripetal acceleration, the stress state at every point in the model can be made the same as at the homologous point in the prototype thus eliminating major deficiency in model testing of geotechnical structures.

A2.1 Model Package

The model tests were performed via a Schaevitz Engineering model with B-8-D rotary accelerator located in University of California at Davis. The model is placed in an aluminum container which holds two halves of the model valley simulating the base rock and the adjacent abutments on either side of a fault. The left block is fixed to the container and the other half is allowed to slide simulating a simple strike-slip fault movement. The surface of the model valley are coated with glued coarse sand to prevent possible slippage between soil and the model base rock at the interface. A specially designed rubber "O" ring seal was installed along the fault line to prevent the leakage of water impounded in the reservoir through the fault itself.

The movement of the block is activated by an air piston positioned below the base rock. The piston is connected to a pneumatic drive system specially designed for this research. The pneumatic drive system is composed of a pressurized cylinder fitted with charging and discharging valves, a solenoid valve and high pressure tubing connected to the piston. The cylinder is charged up to 600 psi through the Schraeder valve, which is always closed except for recharging the cylinder. The discharging valve is always closed except for supplying the pressure to the piston. The cylinder is mounted on a firmly braketed support which is tightened to the centrifuge web. The solenoid valve of normally-closed type was connected between the piston and the cylinder so that the pressure in the cylinder can be hold until loading of the piston is required. A 12 DC volts voltage is required to activate the valve. The valve can handle up to 2500 psi pressure. The movement of the piston can be adjusted to produce a horizontal displacement of the sliding block in the range of 0.1 to 1.0 inch by providing a predetermined distance the moving block is permitted

to travel between the block wall and the bucket wall. This movement is applied suddenly under the control of the solenoid valve.

A2.2 Model Preparation

The soil used for the research is Yolo Loam, a locally available silty clay which can be categorized as CL according to the Unified Soil Classification System. Before use, the soil is air-dried, crushed and processed through a number 40 sieve. The seived soil is moistened with de-ionized water to approximately 20 % water content which is about 3 % wet of the optimum obtained based on the standard Proctor test, a normally employed practise for dam construction. De-ionized water is used to prevent the build-up of ions over time as the soil is reused. In order to get the uniform moisture distribution throughout the soil, the soil is watered via plant-watering spray, and sieved again via number 10 sieve at about 15 % of water content to prevent the wet soil from being crumbled into small lumps. Before the soil is compacted, it was cured in a moisture room for at least 24 hours to ensure uniformity in water content of the soil.

The prepared soil is placed in the sample box evenly by hand to have approximately 2.5 inch thick of loose soil for each compaction lift. The embankment is compacted in four layers. The compacted thickness of each layer is approximately 0.9 inch. During the compaction it is important to maintain uniform compaction effort and lift thickness. Because of the geometry of embankment, the whole earth structure can not be compacted in a usual manner. The compacted area of each layer is reduced from the bottom to the top because of the shape of the embankment. Wooden blocks are used as spacers to fill the reduced area and to support the contained soil firmly so that the soil inside could be compacted as in a rigid model.

The standard Proctor compaction test (ASTM D698) was performed for the sample

soil to obtain a maximum dry density of 111.5 pcf and an optimum water content of 16.7 %. As is often the case in dam construction practice, the placement water content is 3 % wet of optimum, and a 95 % of relative compaction is exercised (i.e. w/c = 19.7 %, γ_d = 107 pcf). The compaction effort of 95 % relative compaction was determined from the calibrated relations of four different cases between the compaction effort and the relative compaction. Every layer was made to experience 1 blow per square inch over the compaction area with a 5.5 pound Proctor compaction hammer dropped 7.60 inch onto the soil.

After the compaction is done, the wooden blocks are removed from the sample. Bacause there is strong contact between the compacted soil and wooden buffers, the removal of blocks needs to be cared in order not to damage the compacted soil structure. It is done by cutting out the adjacent soil by a blade and taking the blocks out together with soil. Then trimming is done to get the proper geometry of the model embankment. The height of the dam is 3.4 inch, the crest width is 0.75 inch, and the slopes of the upstream and downstream are 1:2 and 1:1.75 respectively. The base of the dam is 13.5 inch wide. The dimensions of the dam section are shown in Figure 3. The compacted and trimmed sample is kept in the humid room overnight before testing in the centrifuge next day. On the day of centrifuge testing, lines of white paint parallel to the crest line are drawn on both the downstream and upstream surfaces of the dam. Also, a line of white-head map pins are placed along the crest of the dam. These markers give a visual display of the movement of the dam for TV viewing while testing is in progress as well as for still photos to show the distorted configurations of the dam. Next, the model is brought onto the centrifuge bucket and positioned right above the piston tightly attached to the bucket bottom by four bolts.

Before closing the centrifuge door for a run, water is filled in the upstream

reservoir up to the elevation of 3.0 inch thus leaving a free board of 0.4 inch. A transparent mylar strip is placed along the crest as a shield to prevent overtopping of water due to sloshing in the reservoir, which occurs as the model is being brought up to the desired g-level. The discharging valve of pressurized cylinder is opened and the safety check is then carried out following the UCD centrifuge laboratory instructions. Finally water is sprayed on the sample to prevent the embankment surface from being dried during centrifugation.

A2.3 Testing Procedure

The model is first brought to the proper g-level under which the base rock displacement is to be applied. The model is then kept at that g-level for at least 15 minutes to establish the steady state hydraulic flow condition through the earth dam. The centrifuge is then stopped in order to check if the seepage flow is properly established. The formation of a phreatic line is checked by observing the wet zone of flow exit at downstream toe of the model embankment and the lowering of the reservoir water level. The measured length of wet zone of flow exit is about 1.80 inch and the water level lowered is about 0.25 inch. Water is added to maintain the water level up to 3.0 inch and is again sprayed on the sample surface. After a careful check over the model, the model is again brought up to the desired g-level and kept at that state for 5 minutes to re-establish the equilibrium conditions. A sudden horizontal displacement of known quantity is then applied to the sliding blick. Looking upstream, the right half of the block is moved upstream with respect to the left half.

Models were geometrically of identical dimensions, but tested with different base movements and under different g-levels. The amount of fault movement d at 60 g ranges from 0.2 to 1.0 inches, which is equivalent to 1.0 to 5.0 feet of prototype

base movement. The g-levels of 80 and 100 times gravity acceleration were also exercised for the base movements of d = 0.45" and 0.36" respectively. The variations of given boundary conditions are shown in Table 2 together with the results of crack developments.

Crack patterns appear immediately in the dam, which can be observed via the TV screen. The test is continued further for another 15 minutes to observe if water leakage would take place through the cracks and/or instability of the dam would follow. After the centrifuge test is terminated, the model sample is removed from the centrifuge. Still photos are taken for the tested model embankment to keep a record of the deformed configurations of the sample. Also surface measurements are taken for the displacements along the painted white lines and the white markers at crest level, as well as the extent the failure surface propagated in the embankment. This procedure is performed right after the test to minimize shrinkage of the sample due to moisture loss or the chance of accidental damage. Next, non-soluable white ink is poured into the crack opening to trace the crack surface development inside the embankment. The researcher investigates the white-ink permeated zone and makes sketches of the cracked surface.

A3. RESULTS AND DISCUSSION

The breakage of the embankment occurs as one half of the model valley moves relative to the other half. The model valley includes the valley floor and two valley walls serving as abutments. The crack patterns of all models are similar, while the extent of crack development varies with different amounts of base movement. A typical crack pattern is shown in Figure 4. It was consistent for all the models to show surface cracks in the downstream part of the fixed half (the left side) and the upstream part of the moving half (the right side) separating the damaged model

into three major broken blocks. Figure 5(a) shows that sets of cracks appeared on the surfaces of both sides of the embankment bearing almost identical crack patterns antisymmetrically. The relative movement of two halves of the model valley forces a shear deformation, which gives rise to stresses causing rupture in the soil as it reaches the limit state. The limit state may be reached either by shear failure or by tension failure depending upon the initial stresses and the loading conditions.

A3.1 Idealization of Boundary Conditions

The boundary loading conditions of the embankment subjected to a strike-slip fault movement can be essentially idealized into two major modes. At the embankment base, as shown in Figure 6(a), the shear plane is predetermined along the fault line and the soil has perfect contact with the base rock and the abutment walls. The loading condition at the vicinity of the embankment base would be close to the direct-shear condition. Thus, the boundary loading condition is named as "direct-shear" mode. At the vicinity of the surfaces of embankment, as shown in Figure 6(b), both sides of the abutment are fixed with the embankment. There exists no predetermined shear plane in the embankment, and surfaces of the two sides of embankment are stress-free. Away from the embankment base it may be assumed the loading condition would be due to the relative side movement of abutment walls. Thus, the boundary loading condition is named as "side-shear" mode. When a strike-slip movement is applied, the right side of the embankment tends to rotate with respect to the left side of the embankment. But the rotational tendency is restricted by the base friction and the fixity of the abutment, and in turn the shear force on the abutments would be accompanied by moments yielded by tensile stress (σ_t) and compressive stress (σ_c) in different zones as shown in Figure 6(b). Under this condition, an embankment can be divided largely into four zones of

different stress condition: zones "A" and "C" in tension, and zone "B" and "D" in compression. One evidence of this stress pattern was manifested in the test of the largest base movement so that the observed heave of the middle broken block was slightly rotated relative to the other adjacent blocks. As the model valley experiences strike-slip fault movement, the complex stress field is formed in an embankment due to the combined effects of two idealized boundary loading conditions.

A3.2 Identification of Crack Pattern

Based on the previous idealization of boundary loading conditions, the overall crack pattern can be identified mainly for three different cases. Firstly, near the vicinity of the fault zone, subjected to a "direct-shear" state, the failure is developed due to a large shear deformation applied along the predetermined fault line, and the soil fails in shear. Deep inside the embankment (soil element #1 in Figure 5(a)), the initial confinement of the soil is high enough so that the Mohr's stress circle would lead to failure by shear as shown qualitatively in Figure 5(b). If the initial horizontal stresses, σ_x and σ_y, are assumed to be equal without considering the vertical stress σ_z, then the direction of the failure plane could be almost identical to that of the fault line. This shear failure zone at the base should be continuous across the width of the dam; however, being a shear failure in a wet clayey soil, the slip surface does not open. Furthermore, due to the high water content, the plastic nature of the clay and the heavy overburden of self-weight, this ruptured zone along the fault deep inside the embankment does not create an open leakage channel, even though it is transversely continuous.

Secondly, near the surface of the embankment, the "side-shear" state of loading condition seems to govern. But for the cases of larger base movement the effect of the shear deformation along the fault line also significantly contributes to the

failure pattern, as the shear failure zone is propagating upwards close to the crest. As a relative movement is applied, the soil in zones "A" and "C" in Figure 6(b) may experience tensile stresses mainly from the "side-shear" loading condition and shear stresses mainly from the "direct-shear" loading condition especially in the middle of an embankment. Near the surface in the middle of an embankment (soil element #2 in Figure 5(a)), as previously observed, the opening of the crack is greater than in the left side, and also considerable shear deformations are shown. This indicates that the crack development initiates from the middel portion due to tensile displacement and shear deformation, and propagates to the left. As discussed before, the soils in zone "A" (Figure 6(b)) are subjected to tensile stress due to the rotational tendency resisted by the base friction and the fixidity of the abutment. Being closer to the toe, the tensile zone "A" becomes narrower to the fault line, because the rotational tendency is more resisted by the base friction. Thus, the soils closer to the toe experience greater tensile stress than the soils closer to the crest. The stress state at failure could be qualitatively illustrated as in Figure 5(c). The soil element closer to the crest is subjected to smaller tensile stress so that it could take more shear stress before failure, and thus θ in Figure 5(c) becomes larger (i.e., the crack develops in the direction 45° or less counterclockwise from the fault direction). On the other hand, the soil element close to the toe could take little shear stress before failure so that θ becomes smaller (i.e., the crack develops in the direction less than 45° counterclockwise from the fault direction). Most of the deformation due to the shear seems to occur after the failure state, because the initial normal stresses are small in magnitude so that the failure condition could be reached by small tensile and shear stresses.

For the cases of larger amount of base movement, however, the stress condition at failure would be more complicated near the surface close to the toe. The straight

open crack in the direction parallel to the fault line is developed about 1.0 inch away from the center line to the right. This seems to be due to the slippage at the foundation-embankment interface at the toe area. The toe area with a lower overburden above the foundation has less resistance to a large fault movement at the embankment-foundation interface than the shear resistence of the embankment soil along the fault line. This could be an explanation of the crack pattern close to the toe shown in a plan view, but the three-dimensional development of the open crack at the vicinity of the toe is more complicated. It was observed that the surface crack and the fault line are connected to form a skewed failure plane. This indicates the shear failure zone and tensile failure zone are combined together in the process of sliding on the foundation interface at the toe, which is a situation taken place after the failure state. Also, the relative elevation difference between the slided blocks at the toe area could be regarded as another cause to create a skewed failure plane.

Thirdly, as the base movement is applied further from the failure state, the opening of the tensile crack in the middle of an embankment grows bigger as the broken parts are splitted apart and translated further. Consequently, the soil element near the surface area along the diagonal crack (soil element #3 in Figure 5(a)) is subjected to the maximum tensile stress in the direction 45 clockwise from the fault direction. As observed before, the diagonal tensile crack developed to the left of downstream side involves very little shear deformation. The stress state at failure could be shown qualitatively as in Figure 5(d). The direction of the subsequent crack propagation is perpendicular to that of the maximum tensile stress (i.e., 45° counterclockwise from the y-axis). But the direction of the opening is identical to that of fault movement, which is shown by the evidence that the discontinuity of the lines drawn on the surface of a model embankment is aligned with

the transverse direction because the movement is laterally constrained by both sides of abutment walls. Also, a series of diagonal tensile cracks are observed when the base movement is large. This seems to indicate that the shear failure zone along the fault line propagates upward progressively, as the base movement is increased, and accordingly the tensile failure zone is transmitted to the higher level. The travel distances of the tensile failure cracks in the test of the largest base movement are shorter than those corresponding ones in other tests. This could be, in the author's opinion, because some of the shear energy is transferred to the higher level as the shear failure zone along the fault line propagates upwards. Another interesting observation from the test is that the propagation of the highest diagonal tensile crack initiates much closer to the center of the dam and extends very limitedly to the left side of the upstream embankment, which is the compressive zone "D" in Figure 6(b). The compressive stress state in the zone prevents the tensile crack from propagating further, but instead, it forces the crack to open wider and deeper, as a larger fault movement is applied. For the models tested, this condition kept the tensile cracks in zone "D" close to the crest and above the water table so that water flow did not occur through the crack openings.

The fracture of the above tension failures is of brittle type with little prior plastic deformation. The crack surfaces are open, and look sharper because little slippage occurred along the surface. The cracks at the base do not impose any immediate threat to water leakage. But the tensile cracks on the surface are indeed troublesome, if they extend to the water level or below. Due to the low level of confinement at the surface and the openness of the tensile crack, the ruptured zones, if transversely continuous, are highly susceptible to erosion.

It is also regarded worth while mentioning about the shrinkage crack observed at the base of the dried sample. As shown in Figure 6(b), block "A" tends to be fixed

with the abutment wall while blocks "B" and "C" move relative to blocks "A" and "D", thus some part of block "A" should experience open crack or corresponding shear deformation, depending on the stress state or the location, to accomodate the relative displacement of the two blocks of the model valley. It seems that the soil below the tensile crack zone further inside the embankment is subjected to a relatively large shear deformation, and in turn the soil experiences a reduction of strength. This weakened zone seems to be indicated by the shrinkage crack shown on the foundation interface of the dried sample. It is evident that this crack was not developed during the test, because the trace of the white ink inside the open crack was not detected all the way down to the bottom.

A3.3 Overall Stability Evaluation: Parametric Study

Based on the test results, the catastrophic release of water through the crack opening is not likely an immediate threat to the model embankments, because the tensile failure surfaces are not transversely continuous, and the shear failure zone in the transverse direction does not create an open leakage channel. In any event, however, a dam experiencing any sizable amount of fault movement in the foundation should always be considered to be critical. Emergency steps should be taken to empty the reservoir in order to alleviate any possible long term and short term danger. In this regard, there comes up a necessity of guideline to evaluate the "transient" safety of the damaged embankment.

According to the previous interpretations on the crack patterns of the damaged model embankment, the threatening is the tensile crack zone, while the zone of shear failure along the fault line is of less concern. As discussed earlier, on the left side of the downstream embankment surface the tensile cracks are developed approximately 45° counterclockwise with respect to the direction of fault line, and in

the middle of the downstream embankment surface the tensile cracks are developed in the direction less than $45°$ counterclockwise from the fault direction. This crack pattern forms the three major broken parts of the damaged embankment. And a safety evaluation of the damaged embankment should include the possibilities if the tensile cracks on both sides of embankment would be continuous, and if water would leak through the open tensile cracks extending to the other side of the embankment. In this sense, the width of middle broken block at the crest appears to be a very significant variable to evaluate the overall safety of a damaged embankment. The width of the middle broken block at the crest of a damaged embankment can be indirectly represented, as shown in Figure 5(a), by ℓ, the length between the toe center to the intersection point of the major diagonal tensile crack and the center line of the embankment. ℓ is the length measured from the left side of the downstream embankment and projected on a horizontal plane. The safety against the possibility of continued tensile cracks in transverse direction can be represented as

$$\ell < nH$$

in which n is the slope of one side of embankment and H is the height of embankment as shown in Figure 3.

In consideration of the possibilities of water flow through a tensile crack opening, some marginal length for the propagation of tensile crack should be reserved so that the tensile cracks may not extend to the other side of the embankment, i.e.,

$$\ell < nH - mB$$

in which m is an empirical coefficient to indicate propagation extent of the major diagonal tensile crack (i.e., $m = \ell_t/B$).

As shown in Figure 5(a), ℓ_t denotes the length between the end point of ℓ and the tip of the major diagonal tension crack projected to the center line on a horizontal plane. And B is the width of an embankment in transverse direction. This relation

can be expressed in terms of B, so that

$l < n(B-b)/(n+n') - mB, (B = (n+n')H+b)$

in which b is the width of the crest, and n' is the slope of the other side of embankment as shown in Figure 3.

Since $B \gg b$, the above relation can be expressed in a more useful form:

$l/B < n/(n+n') - m$

Figure 7, shows the relationship between l/B and the amount of fault movement (d) together with the relationship between $(l + l_t)/B$ and d. One can recognize that the difference of these two curves denotes the empirical coefficient (m), which is also plotted with respect to d/H in Figure 8. It is interesting to see in Figure 7 that, as d increases, the value of $(l + l_t)$ initially increases almost in a linear fashion and gradually converges to a certain level. This is because, while l increases continuously, m increases initially to a maximum and tends to decrease until l_t becomes zero as shown in Figure 8. As discussed earlier, the propagation of tensile crack is limited as it extends into the compression zone, thus the peak of the curve indicates the transition point from which the diagonal tensile crack extends to the compression zone. This finding is very useful to evaluate the safety of an embankment. One can perceive that the free-board could be set based on Figure 7 so as to keep the water table below the development zone of tension crack for an embankment to be subjected to a predicted amount of fault movement. Also, it is easily understood that the embankment of greater height (or higher free-board) is in a safer side than the one of smaller height.

For the purpose of safety evaluation, it is proper to choose m value for the case that the tensile crack propagates close to the dam crest without extending to the compression zone (i.e., the case of d/H when $(l + l_t)$ is equal to nH). From Figure 7 and Figure 8 the m value for this condition is about 0.28, which is also

the value of the maximum of the curve. In this regard, m is suggested to be 0.28 from the model tests. However, the m value seems to be influenced by L (length of crest in longitudinal direction) and H (height of embankment), and more tests with larger L and H values via a larger centrifuge can draw a more comprehensive conclusion. The above equation together with Figure 7 incorporates the variables of amount of fault movement, embankment geometry, and the propagation extent of tensile cracks. This set of information can be used as a guide line to evaluate the propagation extent of tensile cracks with regard to the dam geometry (i.e., crest level and the free board, etc), thus to evaluate the "transient" safety for a given geometry of embankment subjected to strike-slip fault movement.

A4. CONCLUSIONS

It is believed, in the long run, the solution of the problem of dam breakage due to fault movement should not be how to withstand a catastrophic accident imposed by fault movement without failure but rather how to avoid or minimize the potential hazards. A centrifuge model study has been reported on the response of earth embankments subjected to fault movement. The fundamental failure mechanism and crack patterns have been identified. A functional relationship has been developed based on the results of the centrifuge model tests relating the amount of fault movement, the embankment geometry and the crack propagation extent in earth embankment. Followings are the conclusions drawn from the centrifuge model study:

1. The crack development on both sides of the embankment bear almost identical patterns antisymmetrically separating the model into three major broken blocks. The surface cracks are not transversely continuous, thus causing no leakage of water.

2. Crack development in earth embankments subjected to a "strike-slip" fault movement shows two major patterns: shear failure deep inside the embankment and

tension failure near the surface.

3. Near the vicinity of the fault zone, the shear failure zone develops along the predetermined fault line and propagates to a higher level. The shear failure at the base is continuous across the entire width of the dam but allows no open leakage channel.

4. Tension cracks develop near the surface of the embankment, but disappear deep inside the embankment. Away from the middle of embankment the tension cracks develop in the direction approximately 45° with respect to the base movement direction, while in the middle they develop in the direction less than 45° from the fault direction. But the direction of the opening is identical to that of the fault movement because the movement is laterally constrained by both sides of abutment wall. Being a tension failure, the crack surface is open and sharper because little slippage occurred along the surface.

5. As the diagonal tensile crack extends to the other side of the embankment, the propagation is restricted by the compression zone, which is formed as a result of the rotational tendency of the model valley being subjected to the relative side movement, and in turn the crack opens wider and deeper as a larger fault movement is applied.

6. A functional relationship has been established based on the model study incorporating the variables of fault movement, embankment geometry, and propagation extent of the diagonal tensile crack. This set of information can be used as a guide line to evaluate the "transient" safety of the damaged embankment subjected to a strike-slip fault movement.

The above discussion and parametric study are only based on the models studied, which are much simplified. A variety of important parameters, which will affect the pattern of crack development, have been left out from this study; the shape(broad or

narrow), the type (zoned or homogeneous), the size of the embankment, and the direction of fault movement, etc. Therefore, the results should not be generalized to reflect the responses of different types of dam under different conditions. Nevertheless, this study does bring up the focus of an important problem which has long been neglected for the overall safety and reliability of an embankment subjected to fault movement.

PART B : NUMERICAL MODEL STUDY

B1. INTRODUCTION

When the fault movement is triggered at the base level of the embankment, soil elements experience elastic and plastic deformations progressively before reaching the critical failure condition. Since the current version of the 3-D FEM code assumes that soil element is maintained as a continuum in the deformed configuration, it does not have the capability to predict the soil response properly beyond the failure of the embankment, i.e., material discontinuity, stress redistribution, material property change, etc. The continuum assumption does not allow the prediction of the soil response beyond the failure condition to be quantitatively accurate. The mechanism of crack development, however, was qualitatively evaluated based on the stress analysis for the deformed soil elements of the damaged earth embankment. The tensile failure zone is identified when the minor principal stress of the deformed soil element is less than zero. The shear zone is identified when the stress state of the deformed soil element is at the point where the critical state line intersects the bounding surface.

B2. MODELING ASSUMPTIONS

B2.1 Undrained Conditions

When a fault movement takes place, the loading is usually applied so rapidly that almost no water flow takes place before loading is terminated. For this reason the loading condition in the saturated soil elements under the phreatic surface can be assumed as undrained for analysis. The traditional simulation of the undrained condition has been to assume incompressibility of the water and the soil

skeleton. Two approaches are commonly used to achieve this goal. One method is to use the special formulation given by Herrmann for incompressible and nearly incompressible solids (Herrmann, 1965), while the other is to use reduced or selective-reduced integration (Zienkiewicz, 1977) for the element stiffness matrix. The first approach was incorporated in the finite element code SAC-3 (Herrmann, 1965); drained and undrained conditions are expressed in a common form to avoid having to deal with seperate formulations. This is accomplished by considering the slight compressibility of the soil particles and the pore water. Thus the pore water pressure is written in terms of combined bulk modulus of the soil particles and the pore water, and results in a very small magnitude of volume change.

For undrained conditions the value of the combined bulk modulus is very large so that the soil behaves as a nearly incompressible solid and care must be exercised to avoid numerical round-off and excessive constraint problems. In this analysis simulation of undrained condition was done by allowing water flow but the effective permeability was set to be zero. Here the effective permeability, which is one of the material parameters, is the term indicating the ratio of the permeability coefficient commonly used in geotechnical engineering divided by the unit weight of water, which in turn is equal to the geometric permeability used in physics divided by the viscosity of water.

B2.2 Initial State Informations

In the application of SAC-3, the time domain for loading history is decided by the user. In the current analysis, a pre-existing gravity field was considered in the model with specified stress conditions of the corresponding proto-type structure. The actual history (e.g., due to "spin-up") of the g-level also can be incorporated by using a "history function" (Mish and Herrmann, 1983). Several preliminary

analyses incorporating a history of gravity showed that the soil elements in the model embankments experienced considerable amounts of deformation after the g-level initialization (i.e., before the base movement was applied). This seems to be mainly due to the fact that the excess pore water pressure generated by the rapid increment of g-level under undrained condition caused the reduction of effective stresses, and consequently a reduction of the shear strength. In order to avoid this initial deformation problem, the stress initialization was set at the 60-g condition. To observe the effect of the fault movement on embankment deformation, it was necessary to separate the loading history into two stages. The application of the gravity field was considered by initializing the stresses and pore water pressure to their proper values; a base movement along the fault.

The initial states of the effective vertical stress, horizontal stresses and pore water pressure are described by means of simple linear equations in the x, y and z coordinates, and are dependent on the locations of the elements. To calculate the effective horizontal stress, a K_o value of 0.5 was assumed for the clay stratum. The value of unit weight of the material was used as 2.347 lb/in^3 (60 times of the submerged unit weight of 67.6 pcf) for specifying the initial stress state, which was established based on the geometry of the embankment shown in Figure 9.

The initial shear stresses were set to be zero. The assumption of zero-value for the shear stresses at the initial condition deserves some comments because shear stresses actually exist in the embankment particularly adjacent to the slope surface. The discrepency in shear stress level in soil elements makes the initial stress state mislocated within a bounding surface, and consequently would induce considerable difference in excess pore water pressure as well as other effective stresses. This assumption will also result in some changes in magnitude and direction of tensile stresses to be developed after the fault movement is applied. This assumption will

also result in some changes in direction and magnitude of tensile stresses to be calculated after the fault movement is applied.

For linear elasticity problems the initial stresses may be taken to be zero, and then the printed stresses are additions to the initial state (i.e., superposition is valid). However, if the bounding surface is used, an accurate initiation of the stress state is extremely important. For this reason the values of the overconsolidation pressure and the initial void ratio are to be specified as "internal variables" for the theory (Herrmann et al., 1980). The void ratio (e_o) was assumed to be 0.8 throught the sample. The value of $e_o = 0.6$ was used for the preliminary run, but $e_o = 0.8$ was found to improve the behavior. This adjustment was made in consideration of the fact that a high e_o leads to a relatively low ultimate shear strength and an increase in positive pore water pressure development under undrained shear condition (similarly an increase in the tendency to compact under drained conditions). The overconsolidation pressure was set to be 12.0 psi for all the elements of the model embankment, which seems to be larger than normal, but it was done on purpose so that the soil elements would be heavily overconsolidated in the surface layer and slightly overconsolidated in the base layer. The bounding surface plasticity soil model has a nice feature that it can account for the strain-softening response by allowing the plastic modulus to be negative.

B2.3 Boundary Conditions

Boundary conditions can be specified in terms of displacement and/or load. For this problem, the specifications were made to simulate an embankment subjected to a transverse base movement at the center of the dam axis. All the specifications were made in terms of displacement. All the boundary nodes located on the interface between the non-moving block (left half) of the embankment and that portion of the

model valley were specified to have zero displacements in x, y and z directions. All the boundary nodes in the moving half were specified with a uniform displacements in the y direction with zero displacements specified in x and z directions. This simulation will consequently deform the elements along the fault by the specified amount of movement (i.e., for elements along the fault, the two nodes on the moving side have the non-zero displacement specified in the y direction, and the two nodes on the non-moving side have zero displacements in all directions). The width of the elements along the center line of the embankment in the transverse direction is relatively small compared to the widths of other elements as shown in Figure 10. The rest of the nodes located on the surface of the embankment are load free.

B2.4 Incremental Analysis

The selection of appropriate time step length is complicated by the nonlinearity of the soil behavior. If consolidation is considered, it becomes more complicated because another factor is involved, i.e., water flow or pore water pressure dissipation. Thus the selection of time steps was decided after a trial-and-error process. The analysis output of the preliminary test showed that most of the elements experienced their ultimate stress levels in the deformed soil elements. An abrupt change in applied loads or displacements will induce numerical stability problems. In a preliminary run, a total of 50 equal steps were assigned throughout the solution history. This of course consumed a lot of CPU time (approximately 15 days via VAX 11/750) to solve the problem completely for the cases of d = 1.0 inch. According to the results of the preliminary tests, solutions for cases of fault movements greater than 0.1 inch were already approached the ultimate values. So, the final analysis was exercised for the solution history of a base movement up to 0.1 inch.

B.3 MATERIAL CHARACTERIZATION

For the present research the material modeled for the numerical analysis was not identical to the material used for the centrifuge tests, but the properties of the material were selected in an attempt to represent the rupture response of the clay embankment. Thus, the purpose of the model calibration for this study was not to fit any existing triaxial data but instead empirically adjusting the model parameters to yield a set of reasonable model parameters of the "artificial" material that would display the desirable stress-strain behavior. The material behavior the author aimed to creat is to exhibit a strain-softening response when the soil elements are subjected to a high deviatoric stress. In order to achieve this goal, at first the preconsolidation pressure is set to be higher than the initial stress level for all the elements of the model embankment so that they would be in a slightly overconsolidated to highly overconsolidated state. Secondly, in the calibration procedure, the model parameters are manipulated to show greater dilation tendency (development of greater negative pore water pressure for the undrained case) for heavily overconsolidated elements. The idea implied in this approach is that the zone of soil elements experiencing a strain-softening response and showing the dilation tendency at failure can be interpreted as the fracture zone. In order to observe from the computer output the development of the negative excess pore water pressure in the soil elements at failure, the initial pore water pressure for all the soil elements were set to be zero.

The bounding surface model, in its most general form, requires the determination of 19 separate constitutive parameters. Two of them are the initial state properties (initial void ratio and maximum past consolidation pressure), and five of them are the material constants which may be obtained directly from simple well-established laboratory experiments. Twelve of them are the model constants which must be

indirectly established through a model calibration process using the results of undraind triaxial tests. Recently, a new form, consisting of a single ellipse, was developed for the bounding surface with 17 parameters. In this study the conventional form was considered, but the recent version can be referred to (Herrmann et al., 1985 and Kaliakin, 1985). The values of the model parameters used in the analysis are tabulated in Table 3.

B3.1 Material Constants

The five material constants in this category are the traditional critical state parameters $(\lambda, \kappa$, M_c and $M_e)$ and the elastic shear modulus G (or alternatively poisson's ratio ν). The values of λ and κ represent the slopes, in e-ln p' space, of the virgin consolidation and swell/recompression lines respectively, for isotropic loading (or alternatively to be obtained from the lines for one-dimensional loading). The values used for λ and κ are 0.05 and 0.02 respectively. The parameter M_c and M_e representing the slope of the critical state line in compression and extension and the values used are 1.0 and 0.7 respectively. The Poisson's ratio ν was used with the value of 0.31.

B3.2 Bounding Surface Model Parameters

Twelve model parameters included in the second category are the surface shape constants R_c, R_e, A_c, A_e and T, the projection point parameter c, the elastic zone constant s, the hardening parameters h_c, h_e, m_c and m_e, and the transition stress P_ℓ (where, in all cases, the subscripts c and e denote the value of the parameter in compression and extension respectively). The values of these parameters can be indirectly obtained through a trial-and-error curve-fitting procedure which utilizes the results of conventional undrained triaxial compression and extension tests.

The surface shape parameter R defines the ratio of the major to minor axes of ellipse 1 as shown in Figure 11. An increase in R causes the point of intersection to occur at a smaller value of I_1 and J_2, and leads to a decrease in the ultimate values of p' and q. In the traditional critical state formulation, R was taken to be a fixed value of R = 2.0 (Roscoe and Burland, 1968), or R = 2.72 (Schofield and Wroth, 1968), regardless of clay type. In the Bounding Surface formulation, R may assume any value in the range $1 < R < \infty$, while values in the more limited range $2 < R < 3$ have been used in the past. In this study the values used for R_c (in compression) and R_e (in extension) were 2.5 and 1.5 respectively.

The surface parameter A controls the shape of the hyperbolic portion of the bounding surface as illustrated in Figure 11. A large value of A results in a relatively "flat" hyperbola and brings the hyperbola further above the critical state line. A small value of A, on the other hand, brings the hyperbola close to the critical state line, as would be appropriate for materials with little or no cohesion. However, since the point of intersection between the hyperbola and the critical state line is fixed, variations in A have no effect on the ultimate shear strenght q_f. Also, an increase in A leads to a decrease in negative pore water pressure developement under undrained conditions (equivalently, a decrease in the tendency to dilate under drained conditions). In theory, A may assume any value in the range $0 < A < \infty$. However, because of the numerical difficulties for too small or too large values, A has been used in the much more limited range of $0.02 < A < 0.02$. In this study the values used for A_c and A_e were 0.15 and 0.135 respectively.

The surface parameter T controls the size of ellipse 2 by defining the point at which it intersects the I_1 axis as shown in Figure 11. The constant T is thus associated with the tensile strength of the material. The precise magnitude of

T is hard to obtain because soil test is hardly performed under tensile stress ($I_1 <$ 0). For a typical soil, T would be restricted to the approximate range $0 < T < 0.2$. However, in all applications to date, T has always been fixed at $T = 0.05$. In this study the value used for T was also 0.05.

The projection point parameter c defines the point along the I_1 axis serving as the center in the radial mapping rule as illustrated in Figure 11. This parameter therefore determines, in part, to which portion of the bounding surface the actual stress point is mapped. The parameter was introduced into the formulation to permit the possibility of initial negative pore water pressure development in lightly over consolidated soils. Variations in c will also alter the degree to which the material tends to dilate or compact. Variations in c never affect the normally consolidated material response, because these undrained stress paths lie on, rather than within, the bounding surface. In theory, c may assume any value in the range 0 $< c < 1$: $c = 0$ places the projection point at the origin ($I_1 = 0$, $J_2 = 0$), while c = 1 places the projection point at the point of intersection between I axis and ellipse 1 (that is, $I_1 = I_o = 3p_c'$). Because very lightly overconsolidated soils normally show a tendency to compact, c will generally have a value in the range $0 < c < 0.7$. In this study the value used for c was 0.0 in order to set the projection center at the origin. This will help later on to figure out the stress state of deformed soil elements adjacent to the origin.

The elastic zone constant s defines the extent of the elastic nucleus and thereby describes the initial yield surface as shown in Figure 11. Because the elastic domain is always within the bounding surface, variations in s never affect the normally consolidated material response. Furthermore, since the elastic nucleus is always centered at the projection point, the influence of s on the response at any given OCR is somewhat dependent on the value assigned to the projection point

parameter c. An increase in s retards the onset of plastic deformation and must therefore result in a stiffer predicted material response. For this reason an increase in s leads to a stiffer stress-strain response, and a decrease in positive excess pore water pressure development under undrained conditions (or decrease in the tendency to compact under drained conditions). In theory the parameter s may assume any value in the range $1 < s < \infty$. A value of s = 1 causes the elastic nucleus to shrink to a point, and thereby permits plastic behavior to occur immediately and throughout. A value of s = ∞ implies purely elastic behavior at all states within the bounding surface, and thereby leads to the prediction of an elastic-perfectly plastic material response. In most applications to date, s has generally been assigned a value of s = 1, since it is the feeling of most researchers that real clays exhibit no purely elastic behavior, but rather experience some degree of plastic deformation even at very low levels of stress and/or strain. A value of s = 2 would be considered extremely large, and numerical difficulties may be observed if the constant assigned a value greater than s = 10. In this study the value used for s was 1.5.

The hardening parameters h and m enter into the equations for the plastic modulus, and thereby control the degree of plastic hardening (or softening) that occurs at stress states within the bounding surface. Of the two constants, h has the more fundamental and significant role. The parameter m was introduced into the formulation solely to ensure that no plastic deformation occurs when $J_2 = 0$ and thereby guarantee a continuous change in plastic modulus as the stress state crosses the I_1 axis (Herrmann et al., 1980). An increase in h and/or m reduces the amount of plastic deformation and must therefore result in a stiffer predicted material response. For this reason an increase in h and/or m leads to a decrease in positive excess pore water pressure development under undrained conditions (or a decrease in

the tendency to compact under drained conditions). However, since the hardening parameters affect the predicted response at stress strates within the bounding surface only, variations in h and m have no influence on the ultimate values of q, p' or u. Variations in s, h and m have nearly identical qualitative effects on the predicted soil response. In theory, h can assume any value in the range $0 < h$, with the degree of plastic hardening increasing with h. A value of $h = \infty$ causes the bounding surface to assume the role of the classical yield surface. Since the model becomes rather insensitive to variations in h beyond a value of about $h \approx 1$, the value of h is typically restricted to the range $0 < h < 1$. In this study the values used for h_c, h_e and h_z were 0.9, 0.72 and 0.5 respectively. In theory, m can also assume any value in the range $m < \infty$, with the degree of the plastic hardening increasing with m. Numerical instabilities (underflow or overflow) may occur if the value of m exceeds the range $0.2 < m < 10$. In all application to date, m has been fixed at the lowest practical value (that is $m = 0.2$), which results in the parameter h being solely responsible for capturing the material's hardening response. In this analysis the value used for m was also 0.2.

The transitional stress p_L represents the mean normal effective stress at which the consolidation curve changes from linear in e-ln p' space to linear in e-p' space. When p_o is not too small and $p < p_l$, variations in p_l only influence the behavior of very heavily overconsolidated soils. An increase in p_l would result in a stiffer predicted material response. For this reason, an increase in p_l leads to an increase in the ultimate shear strength q_f and an increase in negative pore water pressure development under undrained conditions (or an increase in the tendency to dilate under drained conditions). The precise value of p_l is generally not experimentally well defined, since consolidation data is hardly obtained at very low mean normal effective stresses. The value of p_l is typically assumed to be within the range

$0.3p_a < p_i < 1.0p_a$, where p_a denotes the atmospheric pressure. The suggested range of values for p_i was shown to be 4.0 to 15.0 psi (Mish and Herrmann, 1983), and the value used is 6.5 psi.

B3.3 Calibration under Undrained Triaxial Conditions

A set of model parameters characterized and tabulated in Table 3 was employed for predicting the response of the "artificial" material under standard undrained triaxial compression and extension loadings at overconsolidation ratios of OCR = 1, 2 and 6. The initial confining pressure was set to be 120 psi. A strain-controlled loading was applied: compression test - 10 % of axial strain was applied to all 3 cases; extension tests - 6 % and 8 % of axial strain were applied for the cases of OCR = 1 and 2, and OCR = 6 respectively. Figure 12 shows the effective stress paths in compression and extension under undrained triaxial condition. Figure 13 shows the deviatoric stress responses due to the axial strain increment for three compression and three extension cases. Figure 14 shows the pore water pressure generation due to the axial strain applied under undrained triaxial conditions. The negative pore water pressure generation for the highly overconsolidated case (OCR = 6) in compression represents the dilation tendency when the material is close to the failure condition.

B4. RESULTS AND DISCUSSION

The stress calculated from the numerical analysis are the normal stresses (σ_x, σ_y, σ_z), the shear stresses (τ_{xy}, τ_{yz}, τ_{xz}), and the pore water pressure (u). In order to evaluate the failure pattern in the deformed elements, the stress outputs needed to be further analyzed. A post-processor was developed to calculate the principal stresses and the associated directional cosines of the stress tensors for

the deformed soil elements by solving the eigen values and eigen vectors respectively. A modified Jacobi method was implemented in the post-processor.

B4.1 Normal Stresses and Shear Stresses

The variation in σ_x, σ_y, σ_z are remarkable only for the two elements closest to the embankment center, i.e., about 1.0 inch away from the center line of the embankment. And the increments of σ_x and σ_y are much greater than that of σ_z, because the loading was applied along the y-direction. The case of smaller fault movement (d = 0.01 inch) shows almost negligible changes of σ_x, σ_y, and σ_z in the fifth layer, while the case of larger fault movement (d = 0.1 inch) shows remarkable variation.

The variations of shear stresses are quite different from those of the normal stresses. Because the base movement is applied in the y-direction, τ_{xz} does not change at all regardless of the amount of base movement or the location of the element in the embankment, and τ_{xy} increases the most along the center of the embankment. The mode of τ_{xy} variation is such that it is peaked at the center of the embankment and sharply reduced to zero in the element attatched to the abutment. The changes in τ_{yz} are not as great as in τ_{xy}, but the interesting point is that the variation mode of τ_{yz} along the row is almost anti-symmetric between the left block and the right block of the embankment. Because the center elements are stretched along the y-direction, the shear stress along the row in the y-direction in the z-plane should be anti-symmetric with respect to the center element, i.e., τ_{zy} of left side = $-\tau_{zy}$ of right side. Because of the symmetry of the stress tensor, τ_{yz} of left side = $-\tau_{yz}$ of right side. From these figures τ_{yy} seems to be the major contributing agent to the shear failure response, but it can not be directly explained because normal stresses also increased in the elements close to the center

line of the embankment. The identification of a shear failure can be more effectively explained by evaluating the variations of β and (J/I)/N in the deformed elements, which will be discussed next.

The results presented so far can be summarized as follows :

1.   The increases in normal stresses due to the base movement are developed mainly within the range approximately 1.0 inch from the center of the embankment, and developed progressively upward from the base level and extended to the surface level as the amount of base movement increased.

2.   Changes in τ_{xz} are negligibly small regardless of the location of the element or the amount of base movement.

3.   The changes of τ_{yz} are not as significant as in τ_{xy} , but the variation mode along the lateral direction is about anti-symmetrical with respect to the center line of the embankment.

4.   The change of τ_{xy} is the greatest among the three shear stresses. The variation is such that the peak value at the center of the embankment is reduced drastically to a lower level and approached zero near the abutment.

B4.2 Excess Pore Water Pressure

    An overconsolidated clay under drained conditions, in general, tends to expand when subjected to a shear stress approaching failure. Under undrained conditions this volume-increase tendency causes the generation of negative pore water pressure. In this sense, the detection of excess pore water pressuer can be sensed as a clue for evaluating the existence of a shear-failure zone. For the smaller base movement case (d = 0.01 inch), only the first layer expenences negative pore water pressure along the center of the embankment. A larger base movement (d = 0.01 inch) case shows that the zones of negative pore water pressure are developed along the center of the

embankment in all five layers. It can be summarized that the negative pore water pressure is initially localized along the center elements in the base layer, and as the base movement increases, the localization propagates vertically upward to the surface level.

B4.3 Stress Ratio β and Slope Ratio (J/I)/N

The quantity β denotes the stress ratio which is used to measure how far the current stress state of a deformed soil element is from the bounding surface which relates the image stress state $\bar{\sigma}_{ij}$ to the actual stress state σ_{ij} as shown in Figure 15, i.e., $\{\bar{\sigma}\} - \{\sigma_c\} = \beta (\{\sigma\} - \{\sigma_c\})$ The image stress is defined by the intersection of the projection line with the bounding surface. The projection line originates at the projection center and passes through the current stress state. For the current model the projection center lies on the I axis and is located at cI_o (Figure 15). The size of the bounding surface is determined by the current value of I_o. As shown in Figure 15, a value of β greater than 1.0 indicates the stress state σ_{ij} lies inside the bounding surface. The quantity (J/I)/N is the slope ratio which is used to measure how far the current stress state is from the critical state line and relates the slope of the critical state line (N) to the slope of the line (J/I) intersecting the actual stress state (σ_{ij}) and the projection center (σ_c). As shown in Figure 15, a value of (J/I)/N less than 1.0 indicates that the stress state σ_{ij} lies below the critical state line.

These two parameters can describe the actual stress state in a very effective manner, and can indicate whether the stress state is at the failure condition or not. When the stress state is at the intersection between the bounding surface and the critical state line (i.e., $\beta = 1.0$ and (J/I)/N = 1.0), it can be regarded as a failure condition. It has been shown that if the value of β is 1.0, the

corresponding value of (J/I)/N is always equal to or close to 1.0, which means the stress state can be on the bounding surface only along the critical state line. This is because the initial stress conditions of all the soil elements are overconsolidated. If a soil element is normally consolidated, this can not be true (i.e., β = 1.0, but (J/I)/N $\neq$ 1.0). From these observations, β = 1.0 could be regarded as an adequate indicator to identify a stress state at failure for this analysis. The failure condition indicated by the β value is the case of a shear failure. The tension failure is discussed later in the next section.

When the base movement is smaller (d = 0.01 inch), the elements which experience failure are located only in the first layer and along the center of the embankment. On the other hand, that when the base movement is larger (d = 0.1 inch), the shear localization zone propegated to the fifth layer along the center of each layer. As the base movement increases from d = 0.01 inch to a higler level, the zone of β = 1.0 expands vertically upwards. The variation of β along the row in the lateral direction is in general such that β is the greatest at the abutment interface and smallest (β=1.0) at the center of the layer. From these observations it can be concluded that the zone of shear failure is initially formed along the center line in the base layer, and as the base movement increases, the shear failure zone propagates vertically upwards to the surface level along the center of the embankment.

B4.4 Minor Principal Stress

A soil element, in general, experiences a tension failure at low stress levels, because soil is extremely weak in tension. The stress states at failure for the tension- stressed soil elements are, in general, situated above the critical state line and close to the origin in the stress invariant space. Within this region the failure criterion employed for evaluating the shear failure zone (i.e., β=1.0 and

(J/I)/N = 1.0) can not be satisfactorily used. Instead, the tensile failure zone can be evaluated more effectively by considering the minor principal stress. When the minor principal stress becomes less than zero, the stress state can be regarded indicating a tension failure.

For the smaller base movement case (d = 0.01 inch) the negative values of minor principal stresses are very small. For the larger base movement case, the variation of minor principal stress is the greatest at the center and decreases very sharply to a minimum within the region of 1.5 to 2.5 inches away from the center and gradually increases as the x coordinate approaches the abutment. This variation shows that for the larger base movement case (d = 1.0 inch), the tensile stress concentrated zone is diverged from the center of the embankment approaching its peak value at an offset of about 1.5 to 2.0 inches from the center. Figure 16 shows the tensile stress concentration at the surface level in a plan view. The curve showing the propagation pattern of the tensile failure is qualitatively drawn interpolating the data points obtained from the computer analysis. Because of the assumptions of a continuum analysis and the limitations on the number of elements, the stress variations are roughly shown, but it is fairly helpful to indicate the tensile failure pattern. Another interesting observation is that the tension stress concentration is the greatest at the surface level and smallest at the base level. This means that the tensile failure propagation starts from the surface level and proceeds inside of the embankment. The propagation depth of tensile failure increases in reality as the base movement increases, but in this analysis this was not shown clearly.

B5. CONCLUSION

The fundamental mechanism of crack development has been qualitatively evaluated based on the stress analysis for the deformed soil elements. The stress conditions

were evaluated from the output data of SAC-3 in which the bounding surface plasticity soil model was employed. A shear failure is identified when the stress state is at the intersection between the bounding surface and the critical state line. A tension failure is identified when the minor principal stress of the deformed soil element is less than zero. The crack pattern observed in the centrifuge model is qualitatively substantiated by the stress analysis for the numerical simulation. The zone of shear stress concentration is initially formed along the center line in the base layer parallel with the base movement direction, and as the base movement increases, the zone propagates vertically upward to the surface level still maintaining the direction along the center of the embankment. The tensile stress concentration zone at the surface level tends to propagate away from the center line of the embankment as the base movement increases, and the propagation starts from the surface level and proceeds inside of the embankment.

From the identified crack pattern based on the computer analysis, one can recognize that the shear-failure zone and the tension failure zone develop separately, i.e., the shear failure propagates from the bottom to the surface level along the center line, but the tension failure propagates from the surface level to the bottom diverging from the center line. For this reason, the two failure surfaces may or may not intersect with each other. The centrifuge model tests showed both possible cases. When a larger amount of base movement is applied, the two failure planes in general intersect with each other.

The other point to be noted from the computer analysis is that at the surface level two failure situations may occur at the same time. This is, in the author's opinion, due to the continuum assumption of the analysis. The tensile failure would be predominant at the surface level, because the tensile failure starts from the surface and the shear failure starts from the base. The separate initiation of two

different failure zones cause the stress redistribution in the embankment as the cracks propagate, and the shear failure would not extend vertically beyond the tensile crack zone.

Followings are the summarized conclusions drawn from the numerical analysis:

1. Significant increments of σ_x and σ_y due to the base movement occur mainly within the range approximately 1.0 inch from the center of the embankment in the longitudinal direction and develop progressively from the base level to the crest level, as the amount of base movement increases.

2. Changes in τ_{xy} are the greatest among the three shear stresses, and the variation is such that the peak value at the center of the embankment gets reduced drastically approaching to a zero-value close to the abutment. Changes in τ_{yz} are not as significant as in τ_{xy} but the variation along the lateral direction is almost anti-symmetrical with respect to the center line of the embankment. Changes in τ_{xz} are negligibly small.

3. Negative pore water pressure is initially localized along the center elements in the base layer, and as the base movement increases, the localization propagates to a higher level.

4. The shear failure zone (zone of $\beta = 1.0$) starts from the base level along the fault line, and propagates up to the surface level as the base movement increases.

5. The tension failure zone at the surface level tends to propagate downward, diverging from the embankment center and disappear deep in the embankment.

6. The shear failure zone and the tension failure develop separately, i.e., the shear failure propagates from the bottom to the surface level along the center line, but the tension failure propagates from the surface level to the bottom away from the center line of the embankment. For this reason, the two failure surfaces may or may not intersect each other. When a large amount of base movement is applied, the two

failure surfaces would intersect each other.

In conclusion, as discussed before, the finite element analysis has supplemented the explanations on crack development behavior identified from the results of the centrifuge model tests. Due to the continuum assumption in the current analysis the prediction of the crack pattern was not quantitatively but qualitatively evaluated based on the stress analysis for the deformed soil elements of a damaged earth embankment.

REFERENCES

1. Anderson, E. M., "Dynamics of faulting and Dyke Formation," Oliver & Boyd, Edinburgh, 1951

2. Bell, F. G., "Fundamentals of Engineering Geology," pp 137-155, 1983

3. Bennett, W. J., Private Communication, California Department of Water Resources

4. Blyth, F. G. H., Freitas, M. H., "A Geology for Engineers," Edward Arnold, pp. 151-155, 1984

5. Cheney, J. A. and Whitman, R. V., "Workshop for Development of Specifications for a Ground Motion Simulator for Centrifuge Modelling in Geotechnical Engineering," held at M.I.T. Endicott House Pedham, Massachusetts, June 6-7, 1983, pp. 31-43.

6. Cheney, J. A. and Fragazy, R. J., "The Centrifuge as a Research Tool," Geotechnical Testing Journal, GTJODJ, Vol.7, No.4, Dec. 1984, pp. 182-187

7. Clark, G. B., "Geotechnical Centrifuges for Model Studies and Physical Property Testing of Rock and Rock Structures," Colorado School of Mines Quarterly Vol. 76, No.4, Oct. 1981.

8. Craig, W. H., "The Centrifuge as an Aid to the Designer," Proceedings of the Symposium on Recent Advances in Geotechnical Centrifuge Modeling, University of California, Davis, July 18-20, 1984, pp. 26-29.

9. Dafalias, Y. F. and Herrmann, L. R.,"Bounding Surface Formulation of Soil Plasticity," Soil Mechanics-Transient and Cyclic loads, John Wiley and Sons, eds., Zienkiewich, O. C. and Pande, G. W. New York, 1982, pp. 253-282

10. Dafalias, Y. F., "Bounding Surface Plasticity. I: Mathematical Formulation and Hypoplasticity," Journal of Engineering Mechanics, ASCE, Vol. 112, No. 9, September 1986, pp. 966-987

11. Dafalias, Y. F. and Herrmann, L. R., "Bounding Surface Plasticity. 11: Application to Isotropic Cohesive Soils," Journal of Engineering Mechanics, ASCE. Vol. 112, No. 12, December 1986, pp. 1263 - 1291.

12. DeNatale, J. S., "On the Calibration of Constitutive Models by Multivariate Optimization. A Case Study; The Bounding Surface Plasticity Model," Ph. D. Thesis, Department of Civil Engineering, University of California, Davis, CA., 1982.

13. Esmiol, E. E., "Seepage Through Foundations Containing Discontinuities," Proceedings of the American Society of Civil Engineers Vol. 83, SM11, Paper 1143, 1957

14. Herrmann, L. R., "Elasticity Equation for Incompressible and nearly Incompressible Materials by a Variational Theorem," AIAA journal, Vol. 3, No. 10, 1965, pp. 1896-1900

15. Herrmann, L. R., Dafalias, Y. F. & DeNatale, J., "Bounding Surface Plasticity for Soil Modelling," Final Report to: Civil Engineering Laboratory, Naval Construction Battalion Center, Port Hueneme, Order # USN N62583-80 M R478, Department of Civil Engineering, University of California, Davis, 1980.

16. Herrmann, L. R., Dafalias, Y. F., and Denatale, J. S., "Numerical Implementation of a Bounding Surface Soil Plasticity Model," International Symposium on Numerical Models in Geomechanics/Zurich/13-17 September 1982.

17. Herrmann, L. R. and Kaliakin, Victor, Shen C. K., "Improved Nunerical Implementation of the Bounding Surface Plasticity Model for Cohesive Soils," Final Report to Civil Engineering laboratoryNaval Construction Battalion Center, Port Huenemee, California, Order No. USN N62583/85MT176, Department of Civil Engineering, University of California, Davis November 1985.

18. Herrmann, L. R., Kaliakin, VIctor, Shen, C. K., Mish, Kyran D., and Zhu Zheng-Yu ,"Numerical Implementation of Plasticity Model for Cohesive Soils," Journal of Engineering Mechanics, Vol. 173, No.4, April, 1987.

19. Herrmann, L.R. and Mish, K.D., "Finite Element Analysis for Cohesive Soil, Stress, and Consolidation Problems using Bounding Surface Plasticity Theory," Department of Civil Engineering, University of California, Davis, Research Report for Civil Engineering Laboratory Naval Construction Battalion Center, Port Hueneme, California, Order No. N62583-83-M-T062, September 1983.

20. Langhaar, H. L., " Dimensional Analysis and Theory of Models," John Wiley & Sons, Inc.

21. Mish, K. D. and Herrmann, L. R., "User's Manual for SAC-3, a Three-Dimensional Nonlinear, Time dependent Soil Analysis Code Using the Bounding Surface Plasticity Model," Report to Civil Engineering Laboratory, Naval Construction Battalion Center, Port Hueneme, CA, Order No. N62583-83-M-T062, October 1983.

22. Robert, F. L., Paul,F. K., "Handbook of Geology in Civil Engineering," McGraw-Hill Book Company, pp 44-1 to 44-16, 1983

23. Scott, R. F. and Morgan, N. R., "Feasibility and Desirability of Constructing a Very Large Centrifuge for Geotechnical Studies," Report 760 - 170, Natioal Science Foundation, Washington, D.C., March, 1977.

24. Sherard, J.L., "A Study of the Influence of the Earthquake Hazard on the Design of Embankment Dams," Report submitted to the California Department of Water Resources, July, 1966

25. Sherard, J. L., Cluff, L. S. & Allen, C. R., "Potentially active faults in dam foundations," Geotechnique 24, No. 3, pp 367-428, 1974

26. Sohn, Joonik, "Differential Settlement of Storage Tank Foundation: Centrifuge and Numerical Model Studies," MS Thesis, Department of Civil Engineering, University of California, Davis, CA. 1985.

27. Sterling, H. J. and Ronayne, M. C., "A Centrifuge Modeling Prediction for Landfill Cover Subsidence," Proceedings of the Symposium on Recent Advances in Geotechnical Centrifuge Modeling, University of California, Davis, July 18-20, 1984, pp. 72-81.

28. Sherard, J. L., et al., "Earth and Earth-Rock Dams," John Wiley & Sons, New York, 1963

29. Zienkiewicz, O. C., "The Finite Element Method," 3rd. ed., London, McGraw-Hill, 1977.

Table 1: Embankment Dams in California Located on Active Faults - A Partial List (after Bennett, 1985)

Dam Name	Height of Dam (ft)	Crest Width (ft)	Total Free-board (ft)	Type of Dam	Storage Capacity (acre-ft)	Volume of Dam cu. yd	Year Com-pleted	County	Fault	M.C.E.	Max. Disp. (ft)	Remark
Lake Ranch Dam	38	20	4.5	ERTH	317	5,000	1877	Santa Clara	San Andreas	8.5	-20	Outlet broke during 1906 EQ. dam failed partially.
San Andreas Dam	107	20	10.0	ERTH	18,500	540,000	1870	San Mateo	San Andreas	8.5	-20	1906 break cuts hill between dam & spillway.
Coyote Dam	140	100	26.0	ERRK	24,500	1,130,000	1936	Santa Clara	Calaveras	7.5	15	Some anti-fault features built into the design.
Quail Lake	45	22	2.0		5,600	1,860,000	1967	Los Angeles	San Andreas	8.5	20	Not a jurisdictional dam on Calif-ornia Aqueduct.
Cedar Springs	236	42	23.0	ROCK	73,000	7,900,000	1971	San Bernardino	Cleghorn	.6.5	3	Some anti-fault features built in design.
Calaveras Dam	210	80	22.4	ERRK	100,000	3,461,000	1925	Alameda	Calaveras	7.5	15	Fault near dam only.
Lower Howell Dam	39	18	3.9	ERTH	153	29,600	1877	Santa Clara	San Andreas	8.5	20	
Upper Howel Dam	36	20	4.5	ERTH	243	31,460	1878	Santa Clara	San Andreas	8.5	20	
Lake Temescal	116	60	10.5	ERTH	485	262,292	1869	Alameda	Hayward	7.5	15	
Grant Co. #2 Dam	27	12	8.0	ERTH	600	16,050	1927	Santa Clara	Calaveras	7.5	15	
Harold Dam	30	10	11.5	ERTH	8,200		1891	Los Angeles	San Andreas	8.5	20	
Hershavy Dam	123	20	13.0	HYDE	203,581	500,000	1923	San Diego	Elsinore	7.5	7	Downstream buttress designed for fault offset.

ERTH = Earth Fill Dam, ERRK = Earth and Rock Fill Dam, ROCK = Rock Fill Dam, HYDE = Hydraulic Fill Dam, M.C.E. = Max. Credible Earthquake Magnitude.

Table 2 : Test summary of crack propagation height in the centrifuge model embankments subjected to different amounts of base movement

Test No.	G level	d (inch)	d/H (%)	H_s (inch)	H_s/H (%)	H_t (inch)	H_t/H (%)
4	60	0.20	5.88	0.95	27.94	1.65	48.53
7	60	0.40	11.76	1.63	48.52	3.15	92.65
2	60	0.60	17.65	2.05	60.29	3.40	100.00
5	60	1.00	29.41	2.75	80.88	3.40	100.00
1	80	0.45	13.24	1.50	44.12	3.40	100.00
3	100	0.36	10.59	1.55	45.59	2.85	83.82

d = base movement , H = height of embankment (3.40")

H_s = propagation height of shear crack , H_t = total propagation height of tension and shear cracks

Table 3 : Summary of calibrated bounding surface model parameters

Symbol	Description of Property	Value
λ	Slope of isotropic consolidation line for an e-ln p' plot	0.05
κ	Slope of elastic rebound line for an e-ln p' plot	0.02
M_c	Slope of critical state line in triaxial space (compression)	1.0
ν (or G)	Poisson's ratio (or shear modulus)	0.31
P_l	Transitional value of confining pressure separating linear rebound curves on e-ln p' and e-p' plots.	6.5 psi
P_a	Atmospheric pressure (used for scaling and establishing units)	14.7 psi
Γ	Combined bulk modulus for soil particles and pore water	10^6 psi
R_c		2.5
A_c	Parameters describing shape of bounding surface (compression)	0.15
T		0.05
c	Projection center variable	0.0
s	Elastic zone variable	1.5
m	Hardening parameter	0.2
h_c	Shape hardening parameter for compression	0.9
h_2	Shape hardening parameter on the I-axis	0.5
$n=M_e/M_c$		0.7
$\mu=h_e/h_c$	Ratios of extension to compression values	0.8
$r=R_e/R_c$		0.6
$a=A_e/A_c$		0.9
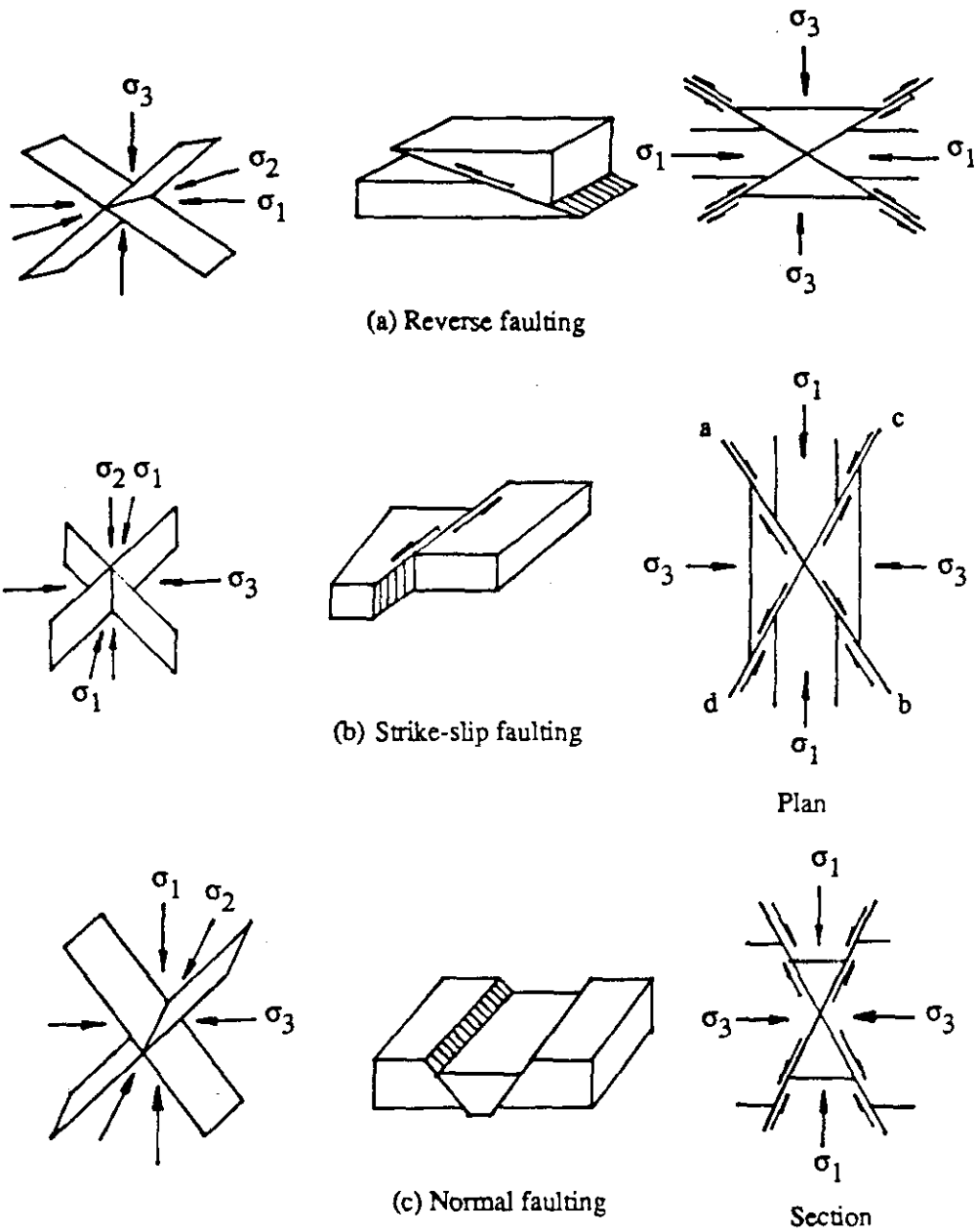
Figure 1: Initial stress distribution causing faulting (after Anderson, 1951) σ_1 maximum, σ_2 mean, σ_3 minimum (compressive) stress. In (a) ab = dextral (clockwise) and cd = sinistral (anticlockwise) displacement
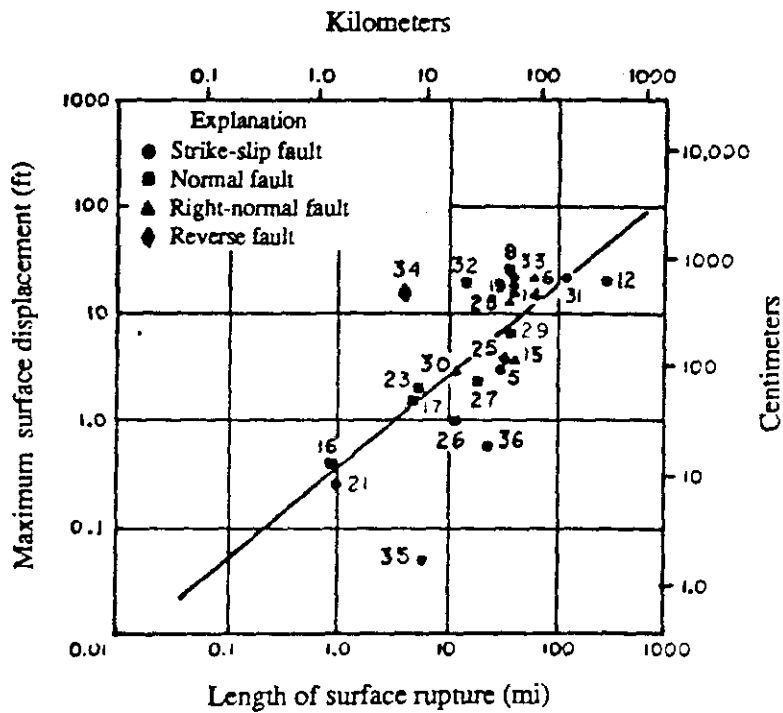
Figure 2 : Rough correlation between length of break and maximum relative displacement of ground on opposite sides (after Bonilla, 1970; numbers on chart refer to individual faults in the Bonilla tabulation)
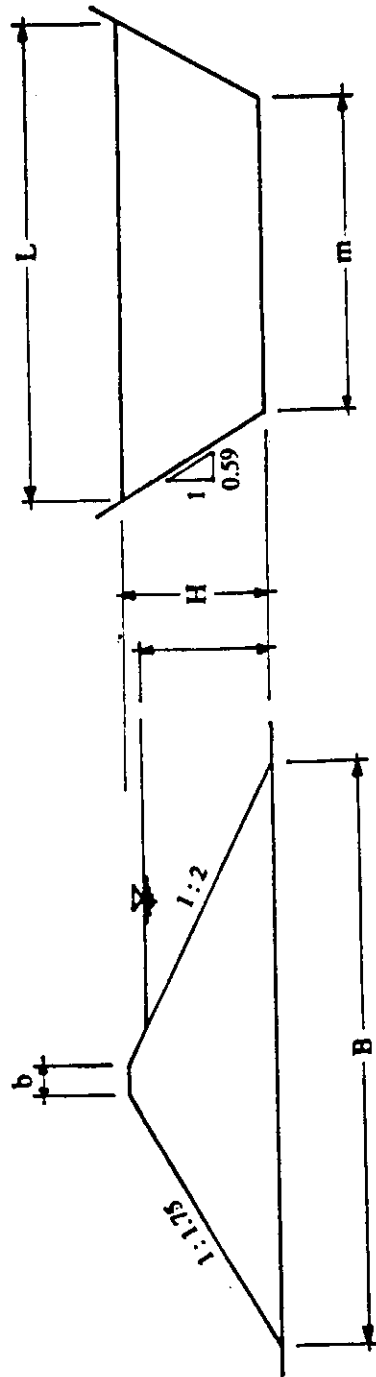
	H	b	B	L	m
prototype (ft)	17.0	3.75	67.50	56.25	36.25
model (60-g) (in)	3.4	0.75	13.50	11.25	7.25

Figure 3 : Dimensions of the model embankment and prototype
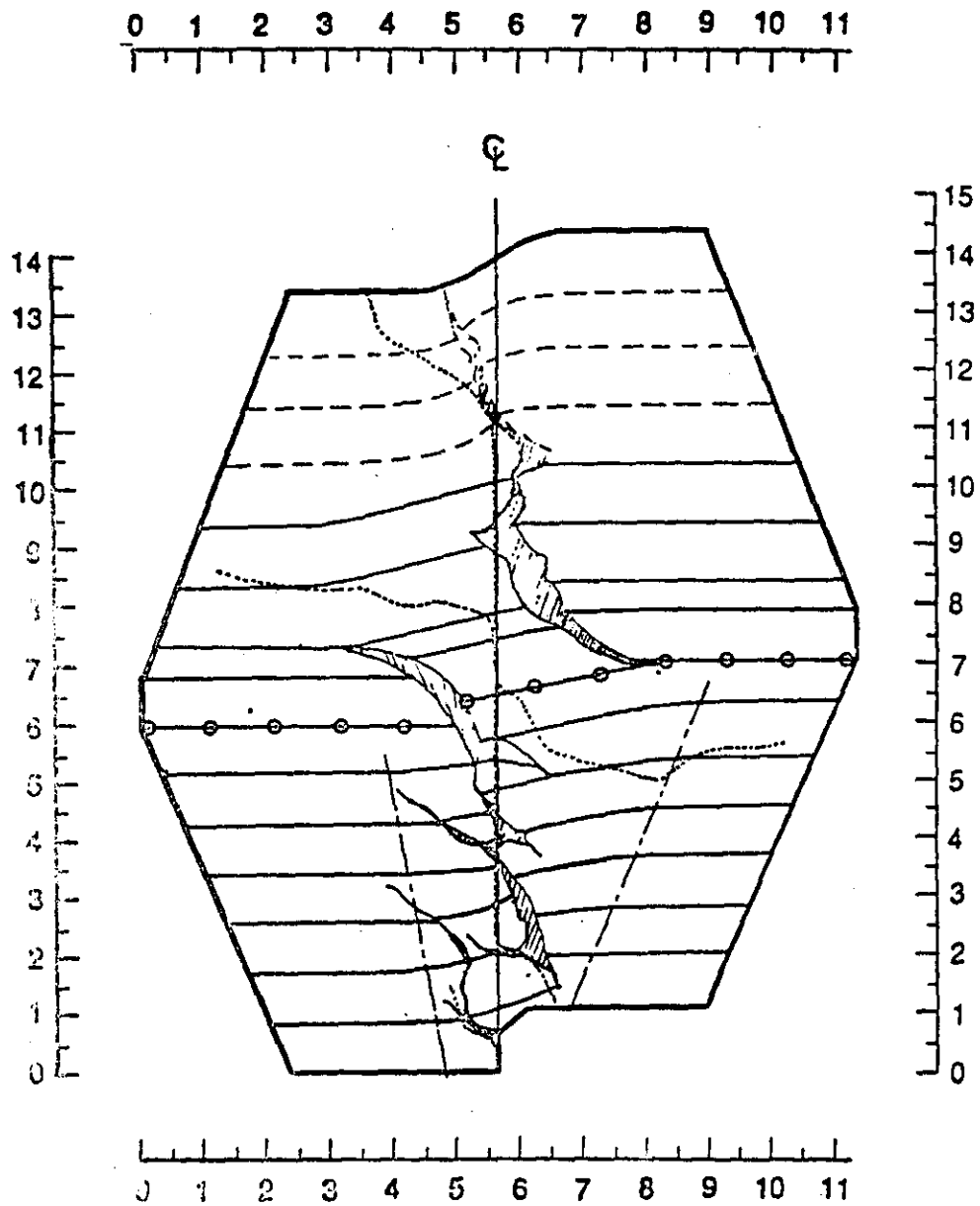
Figure 4 : Plan view of the crack development for the sample #5 (d= 1.00 inch)

(c) tensile failure state of element #2
θ is the angle from y-axis to the tensile failure plane

$2\theta < 90^o, \theta < 45^o$

(d) tensile failure state of element #3
θ is the angle from y-axis to the tensile failure plane

$2\theta = 90^o, \theta = 45^o$
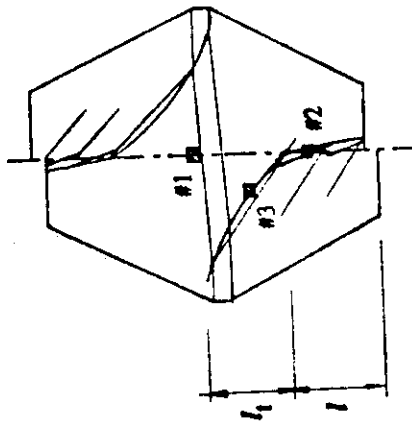
(a) typical crack pattern of a damaged model
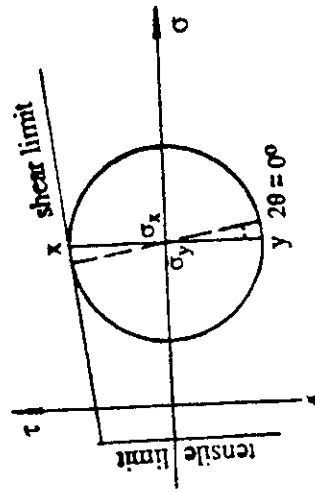
(b) shear failure state of element #1
θ is the angle from y-axis to the shear failure plane
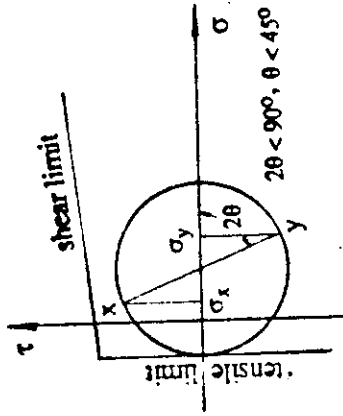
$2\theta = 0^o$
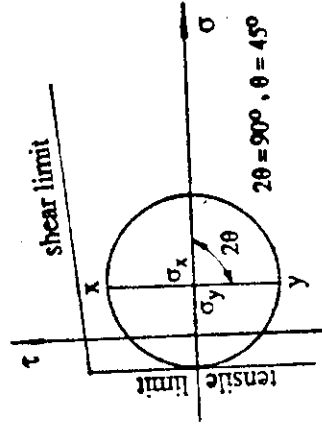
Figure 5 : Typical crack pattern of a damaged model embankment and three failure states
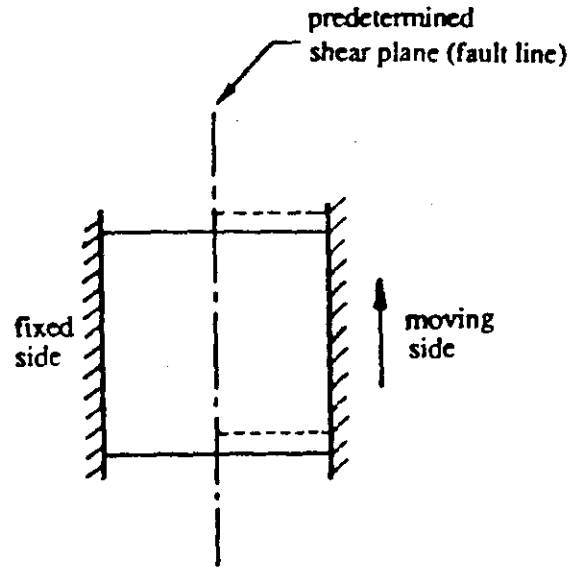
(a) "direct-shear" mode
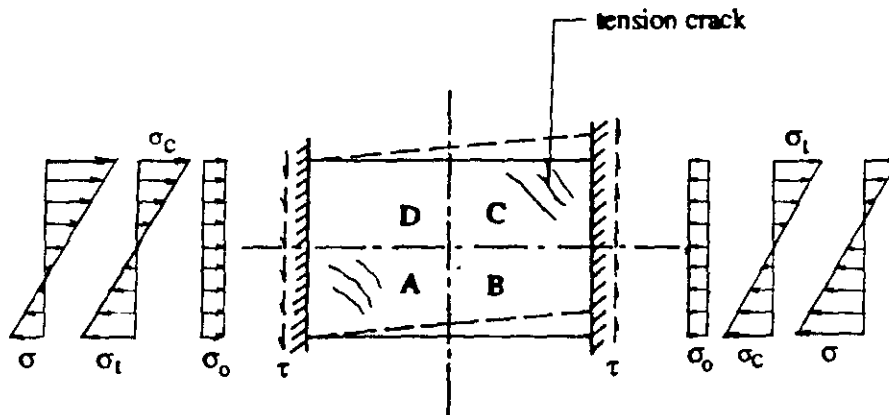
(b) "side-shear" mode

Figure 6 : Idealization of boundary loading condition of an embankment subjected to fault movement; (a) "direct-shear" mode at the base level (b) "side-shear" mode at the surface level
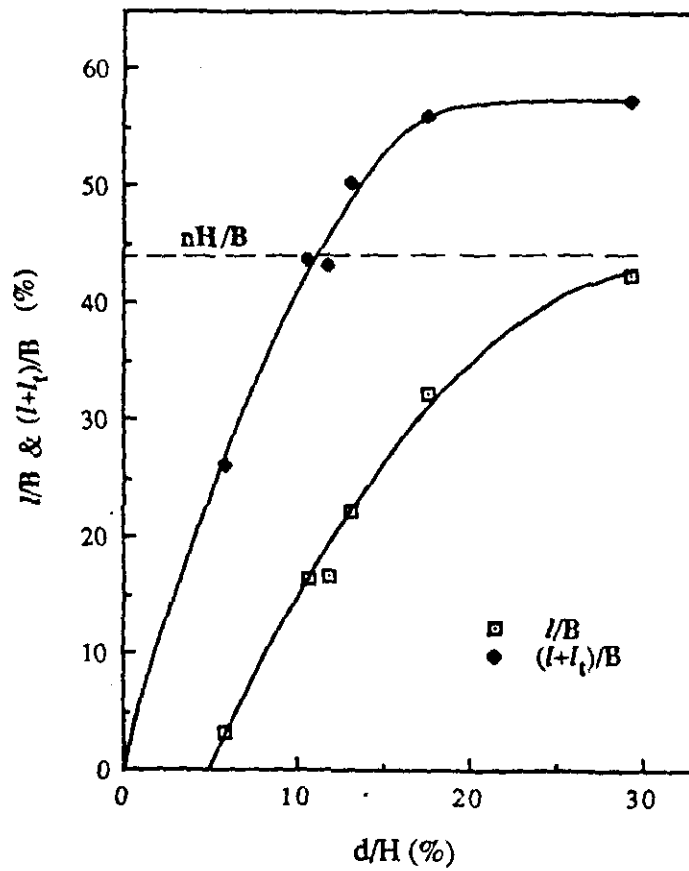
Figure 7 : Functional relationship to evaluate a "transient" safety of the damaged embankment subjected to strike-slip fault movement.
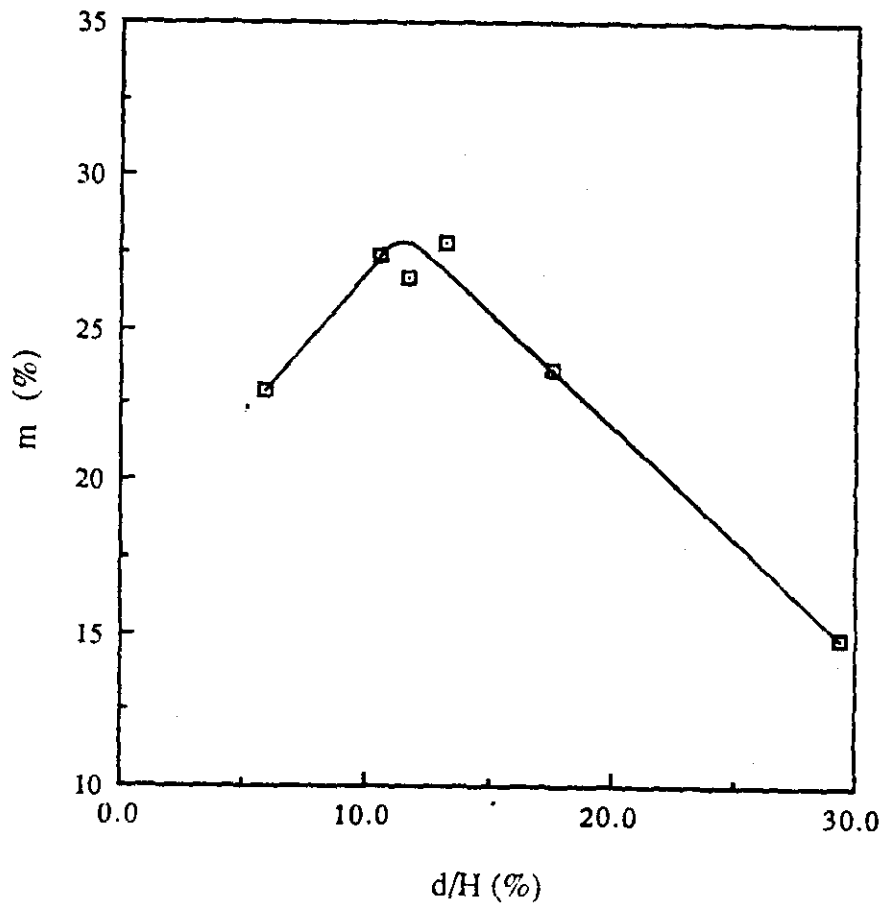
Figure 8 : Empirical coefficient (m) vs. d/H indicating the propagation extent of major diagonal tensile crack
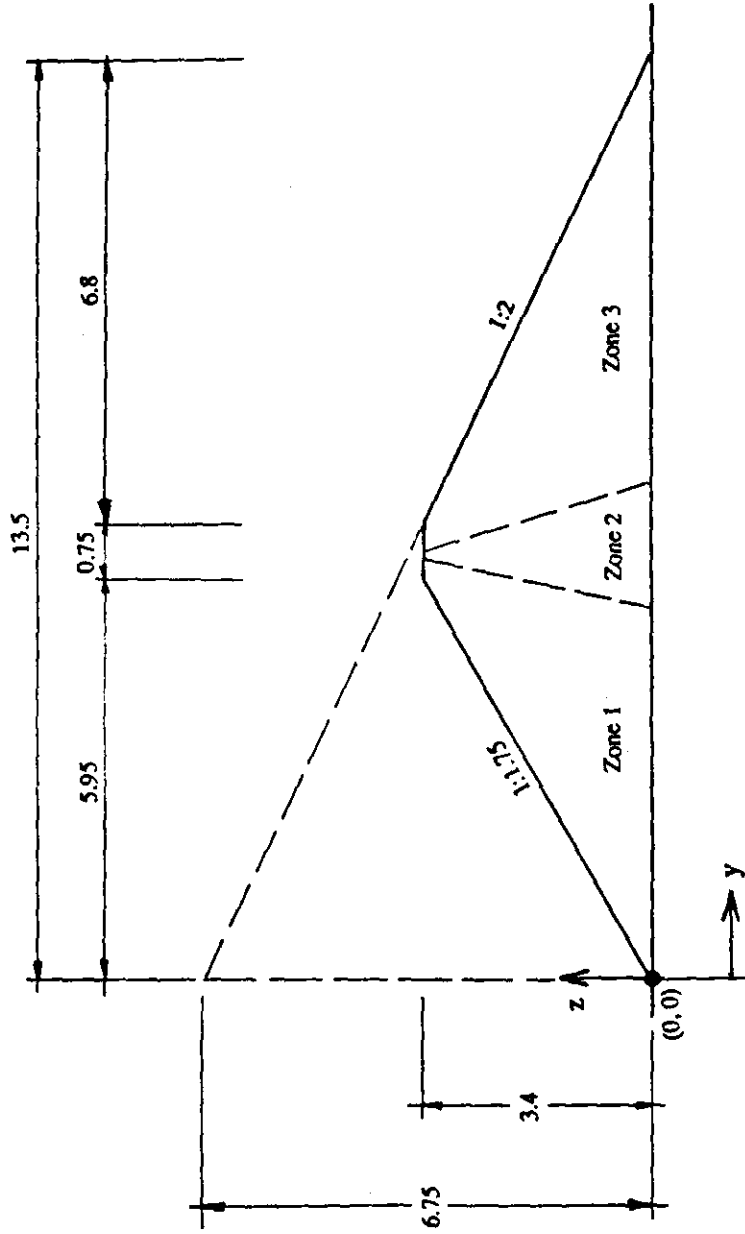
Figure 9: Initial state informations for 3 different zones of model embankment.

Element Number = 405

Node Number = 600
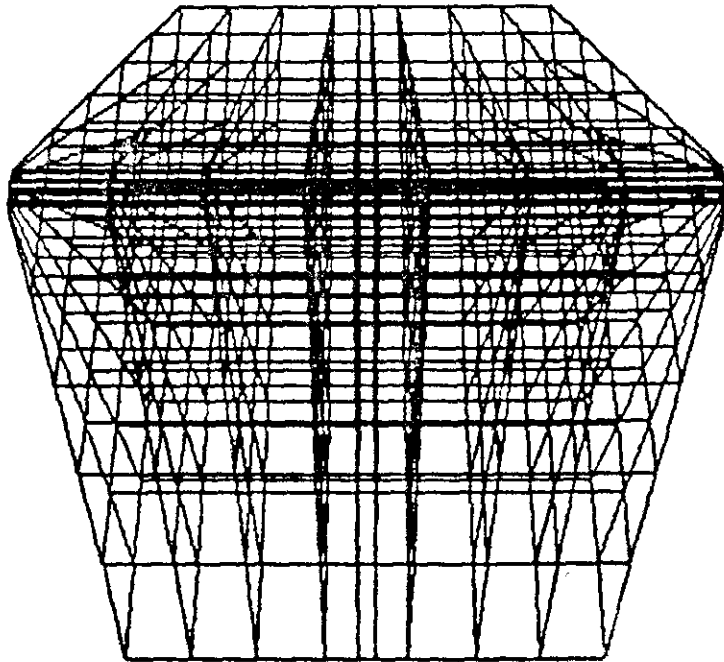
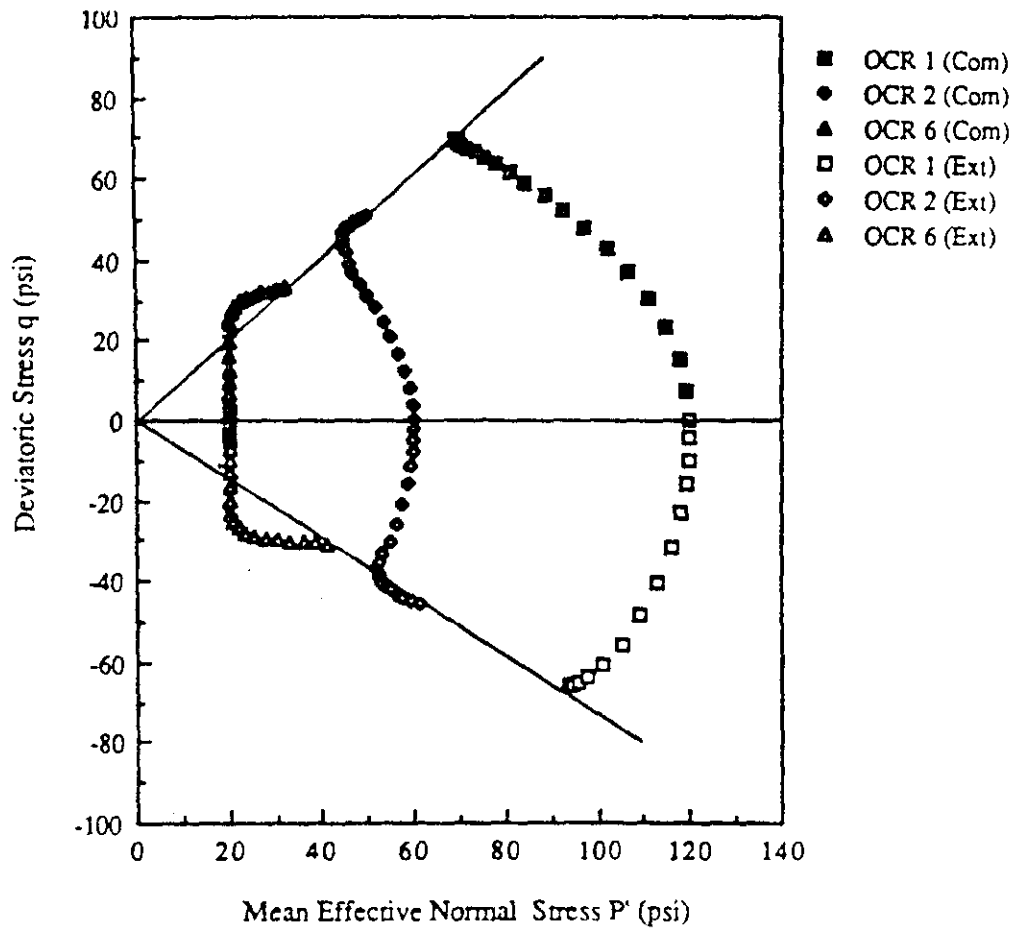Figure 10: The 3-D mesh generation for the embankment subjected to fault movement.
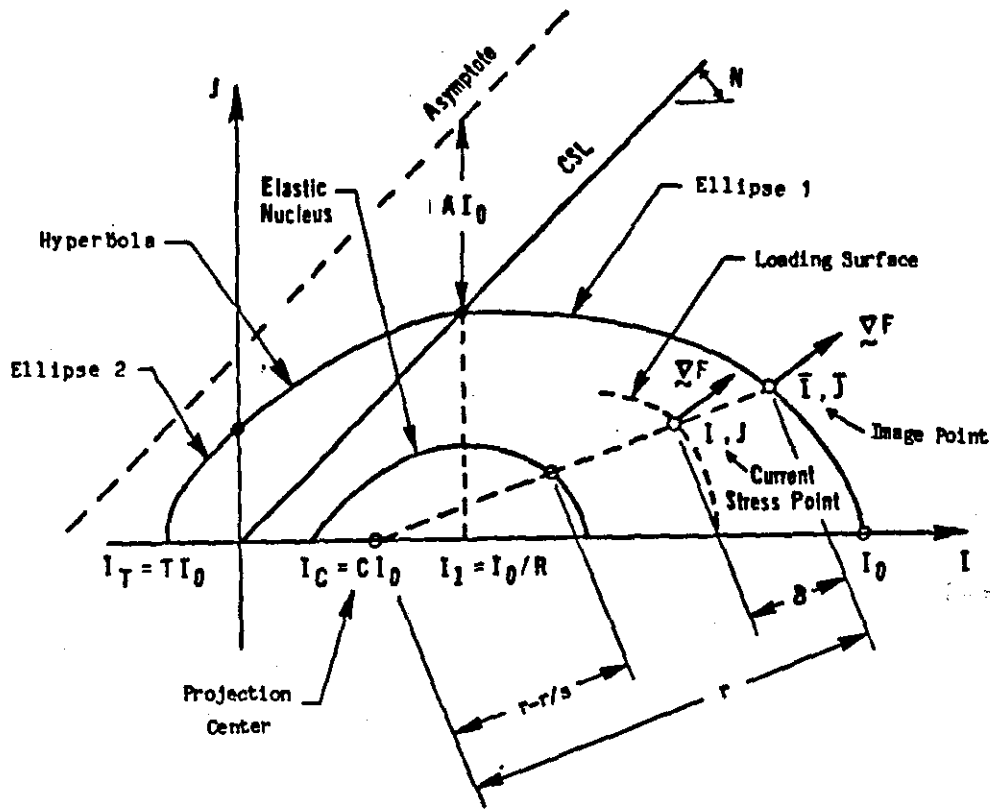
Figure 11: Schematic illustration of the bounding surface in invariant stress space.

Figure 12: A family of stress paths in compression and extension under undrained triaxial conditions.
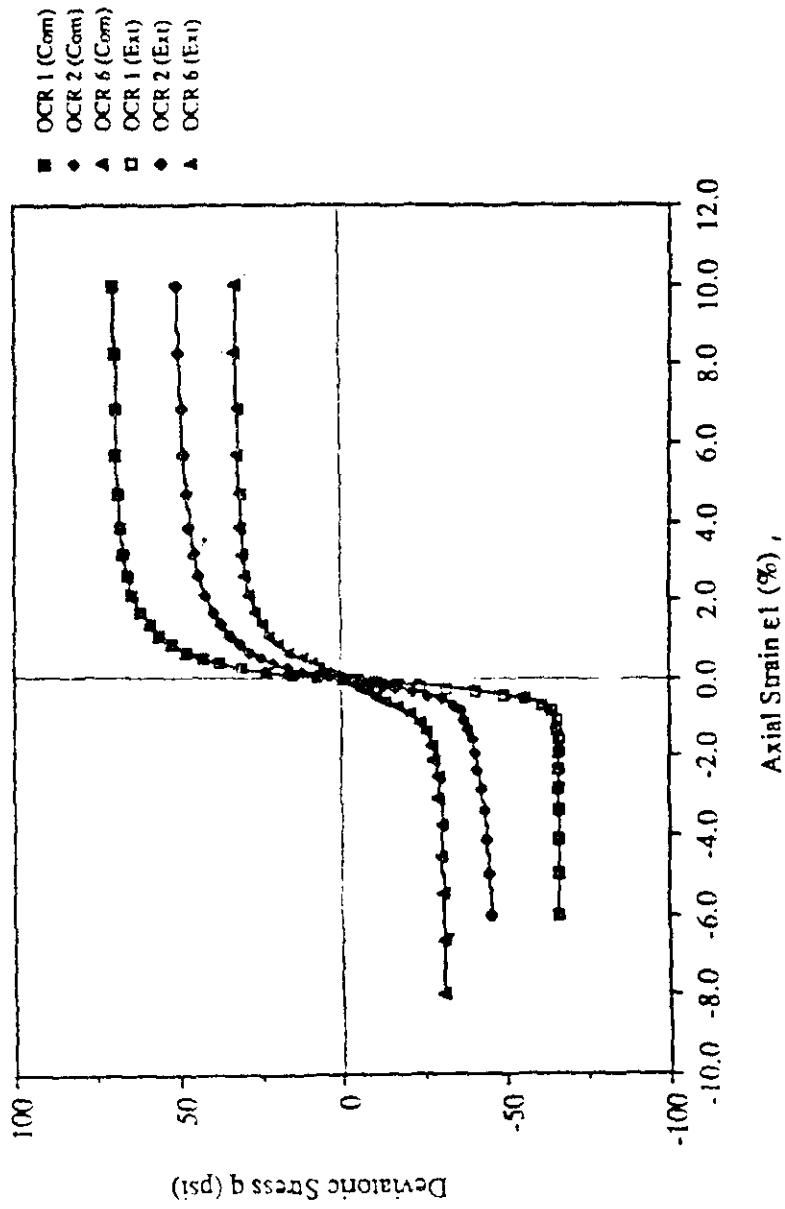
Figure 13: Deviatoric Stress vs. axial strain in compression and extension under undrained triaxial conditions.
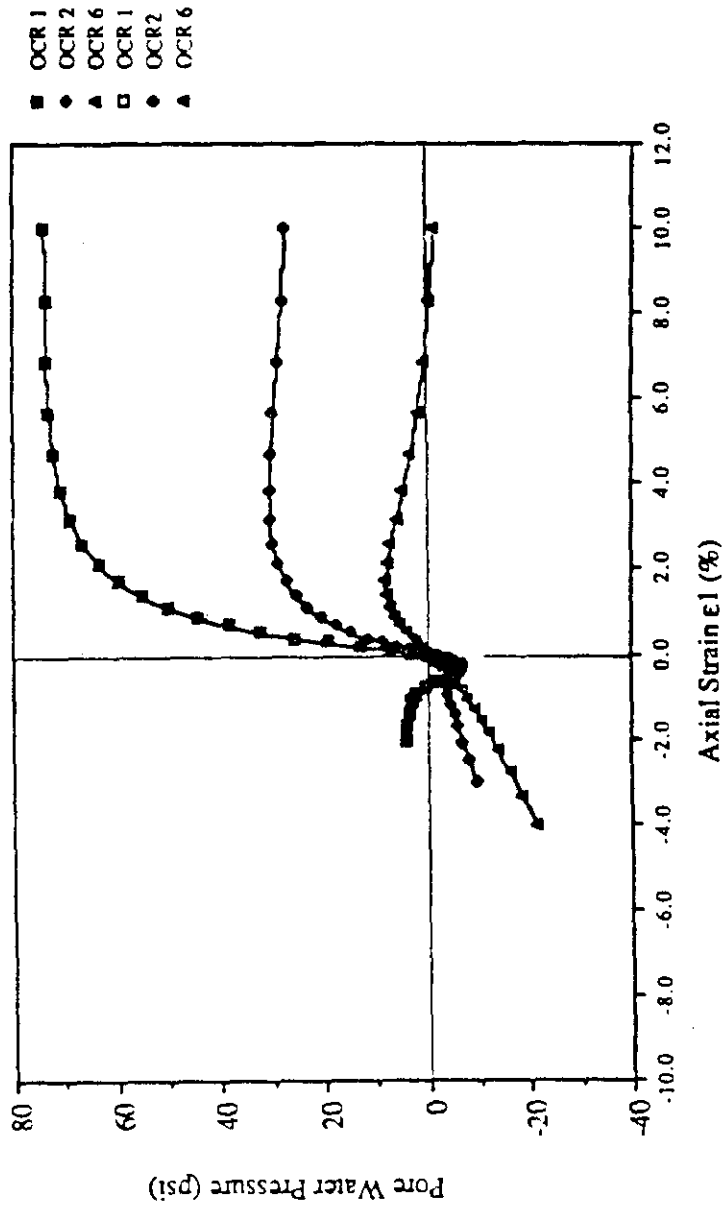
Figure 14 : Pore water pressure vs. axial strain in compression and extension under undrained triaxial conditions.

Figure 15: Cross-section of the bounding surface for cohesive soils in invariant stress space to illustrate the meaning of BETA (β) and (J/I)/N.
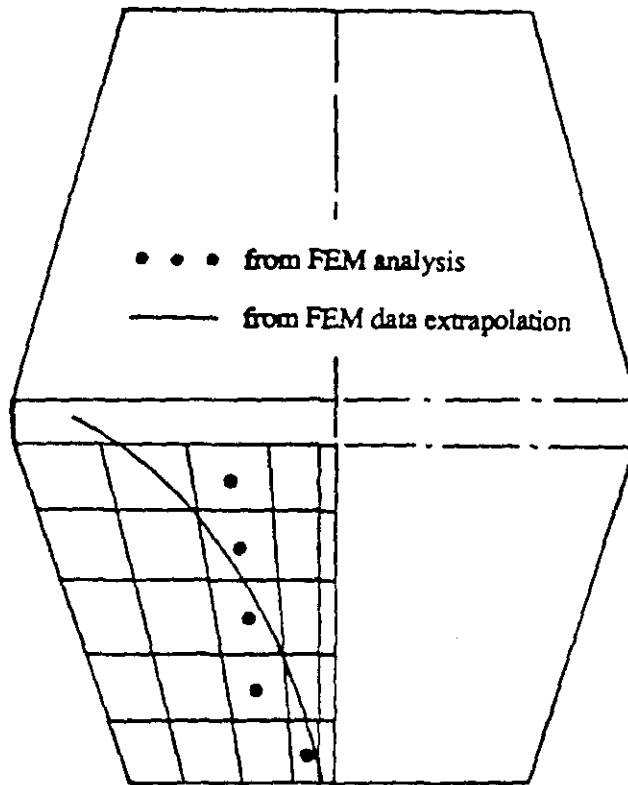
Figure 16: The plan view illustrating the maximum tensile stress zone away from the center of the embankment.